National Technical University of Athens

Postgraduate Studies Program
"Computational Mechanics"

Master's Thesis

Computational modelling of latent heat storage systems with integrated phase change materials in building applications

Nikolaos Ioannou

Supervisor: Prof. Maria Founti

School of Mechanical Engineering, NTUA, Greece

February 2014

Acknowledgements

The specific thesis is presented for the Master of Computational Mechanics, in the National Technical University of Athens. It is elaborated in the school of Mechanical Engineering, at the Laboratory of Heterogeneous Mixtures and Combustion Systems.

I take this opportunity to express my sincere appreciation to my Professor, Maria Founti, for the opportunity she gave me to work in the interesting field of the multiphase computational fluid dynamics.

I, also, wish to disclose my gratitude and deep regards to my supervisor, Doctor Dionisis Kolaitis, for his exemplary guidance, monitoring and constant encouragement throughout the course of this thesis. He suggested the topic of this thesis and provided continuous information in every aspect of this work.

It is important to acknowledge the contribution of Doctor Helmut Weinläder, from the Bavarian Center for Applied Energy Research, Department of Functional Materials for Energy Technology. He provided with information on the characteristics of the experimental validation case. This had a decisive impact on this work. Also, I would like to thank him for the useful information on windows properties.

At this point, I would like to state that this assignment would not be possible to finish, without the heartily support of my friends. I would like to thank especially my dear friend, Vicky Gkloumpou, for her constant encouragement and valuable advice on how to write properly in the English language.

Lastly, I thank my family, which believes in me in every step I take in my life.

Abstract

The purpose of this thesis is to assess the effect of thermal systems, that incorporate phase change materials, with the development of a computational tool.

In the introduction, a brief consideration concludes, that the modern way of life requires large amounts of energy in the building sector, in order to meet the needs of lighting and thermal comfort. The ventilation, heating and air conditioning systems consume more energy, and therefore their performance plays a significant role in saving energy.

A, relatively, new generation of applications can make these systems more efficient. These applications adopt the use of phase change materials. These materials can store energy in the form of latent heat. Thereby, it is necessary to study their behaviour, their advantages and, also, their limitations. In addition, previous works were investigated. This contributed in gaining insight and, also, a valuable fashion to treat the heat capacity: the effective heat capacity method. These topics are discussed in the second part.

The investigated cases in this work, present complicated features: the buildings are heated with thermal radiation, natural convection is observed and multi-layer objects are employed. Hence, the role of the third chapter is to serve as an introduction to heat transfer phenomena and fluid dynamics. It is discussed, that an analytical approach on the temperature and flow fields is impossible. Hence, the computational method of finite volume will close this chapter

The fourth chapter presents the computational study of two cases. Initially, the experimental study of a blind, which integrated a phase change material, is described. Then, the characteristics of the numerical model are presented. Eventually, the results of the simulation show a very good agreement to the experiment, verifying the method.

Furthermore, a new developed system is investigated under two different environment conditions. This system consists of slats, in which an insulation layer and a phase change material are embedded. It will be installed on walls of existing building to improve their thermal characteristics. The results show the beneficial role of the specific applications in the summer period. More tests should be performed to obtain more useful information for winter days as well. In addition, an overview reveals the positive and negative features of this method, and countermeasures are suggested.

Finally, general remarks of this work with comments and overall observations conclude this work. Thermal energy storage systems have, in general, a positive impact and we can gain the

most out of them with careful design. The presented numerical method is considered suitable to simulate heat transfer phenomena and future simulation work is outlined.

Περίληψη

Ο σκοπός αυτής της διπλωματικής εργασίας είναι να εκτιμήσει την επίδραση θερμικών συστημάτων, τα οποία ενσωματώνουν υλικά αλλαγής φάσης, με την ανάπτυξη υπολογιστικών εργαλείων.

Στην εισαγωγή, μια σύντομη θεώρηση καταλήγει στο ότι, ο σύγχρονος τρόπος ζωής απαιτεί μεγάλες ποσότητες ενέργειας στον κτιριακό τομέα, ούτως ώστε να καλυφθούν οι ανάγκες φωτισμού και θερμικής άνεσης. Τα συστήματα αερισμού, θέρμανσης και κλιματισμού καταναλώνουν, ίσως, την περισσότερη ενέργεια, και για τον λόγο αυτό η απόδοσή τους παίζει σημαντικό ρόλο στην εξοικονόμηση ενέργειας.

Μία, σχετικά, νέα γενιά εφαρμογών μπορεί να καταστήσει τα συστήματα αυτά πιο αποδοτικά. Οι εφαρμογές αυτές υιοθετούν την χρήση υλικών αλλαγής φάσης. Τα υλικά αυτά μπορούν και συσσωρεύουν ενέργεια υπό την μορφή λανθάνουσας θερμότητας. Με τον τρόπο αυτό επιτυγχάνεται η θερμοκρασιακή ομοιομορφία. Επίσης, η αποθηκευμένη θερμότητα μπορεί να χρησιμοποιηθεί σε μελοντικό χρόνο. Τα υλικά αυτά, ο τρόπος λειτουργίας τους, καθώς και τα ιδιαίτερα χαρακτηριστικά τους μελετώνται στο δεύτερο κεφάλαιο.

Στις περιπτώσεις που μελετώνται, οι κτιριακές εγκαταστάσεις θερμαίνονται λόγω της ηλιακής ακτινοβολίας. Επίσης, λόγω θερμοκρασιακών διαφορών, παρατηρούνται φαινόμενα φυσικής συναγωγής. Για τους λόγους αυτούς, ο ρόλος του τρίτου κεφαλαίου είναι να λειτουργήσει ως μια εισαγωγή σε φαινόμενα μεταφοράς και ρευστοδυναμικής. Επιπροσθέτως, θα αποδειχθεί, ότι η αναλυτική επίλυση του θερμοκρασιακού και του ροϊκού πεδίου είναι αδύνατη, συνεπώς η αριθμητική προσέγγιση κρίνεται απαραίτητη. Στοιχεία της υπολογιστικής μεθόδου των πεπερασμένων όγκων θα κλείσουν το κεφάλαιο αυτό.

Στο τέταρτο κεφάλαιο, λαμβάνει χώρα η υπολογιστική μελέτη δύο περιπτώσεων. Αρχικά, περιγράφεται η πειραματική μελέτη συστήματος περσίδων, στο οποίο έχει εγκατασταθεί υλικό αλλαγής φάσης. Εν συνεχεία, αναλύονται τα χαρακτηριστικά του υπολογιστικού μοντέλου. Τελικά, παρουσιάζονται τα αποτελέσματα της προσομοίωσης, τα οποία παρέχουν ικανοποιητική συμφωνία με τις τιμές του πειράματος, παρέχοντας πιστοποίηση στο υπολογιστικό εργαλείο.

Στο δεύτερο σκέλος, μελετήθηκε ένα νέο σύστημα, το οποίο αποτελείται από περιστρεφόμενες περσίδες. Οι περσίδες ενσωματώνουν ένα στρώμα μονωτικού καθώς και υλικό αλλαγής φάσης. Εκτιμήθηκε η επίδραση του συστήματος στην θερμική συμπεριφορά εξωτερικού τοιχώματος, υπό δύο διαφορετικές κλιματικές συνθήκες. Τα αποτελέσματα δείχνουν ευνοϊκή επίδραση έναντι σε περιπτώσεις χωρίς την εγκατάσταση του συστήματος. Ωστόσο, προτείνονται συμπληρωματικές προσομοιώσεις και βελτιώσεις στο υπολογιστικό μοντέλο, για την εξαγωγή περαιτέρω χρήσιμων συμπερασμάτων.

Τέλος, γενικά συμπεράσματα και προτάσεις για μελλοντική δουλειά κλείνουν αυτή την διπλωματική. Τα υλικά αλλαγής φάσης παρουσιάζουν θετικό αντίκτυπο σε κτιριακές εφαρμογές, ενώ το υπολογιστικό εργαλείο, που αναπτύχθηκε, δείχνει να έχει δυνατότητες εξέλιξης.

Contents

List of Tables

List of Figures

Nomenclature

Latin

$\dot{q}$	heat flux (W/m^2)
$\mathbf{n}$	unity normal vector
$\vec{V}$	fluid velocity (m/s)
a	absorptivity coefficient
C_p	heat capacity under constant pressure (J/K)
c_p	specific heat capacity under constant pressure (J/kgK)
e	internal energy (J)
F	force (Nt)
g	gravity accelaration (m/s^2)
g_v	g-value of window
Gr	Grashof number
H	enthalpy (J)
h	heat transfer coefficient (W/m^2)
h_{rad}	radiative heat transfer coefficient (W/m^2K)
k	thermal conductivity (W/mK)
L	specific melting enthalpy (J/kg)
L_0	characteristic length (m)
n	number of moles (mol)
Nu	Nusselt number
p	pressure (Pa)
Pr	Prandtl number
Q	heat (J)
r	reflectivity coefficient
Re	Reynolds number
T	temperature (K or °C)
U	overall heat transfer coefficient (W/m^2K)
u_0	characteristic velocity (m/s)
V	volume (m^3)
W	work (J)
w	gas constant $(J/molK)$
w	thickness (m)
X	general displacement (m)

Greek

α	thermal diffusivity (m^2/s)
β	volumetric temperature expansion coefficient (K^{-1})
δ_H	hydrodynamic boundary layer (m)
δ_T	thermal boundary layer (m)
ϵ	emissivity coefficient
λ	bulk viscosity coefficient (Nts/m^2)
μ	dynamic viscosity (Nts/m^2)
ν	kinematic viscosity (m^2/s)
ω	weight factor for transient numerical schemes
Φ	heat source (W)
ρ	density (kg/m^3)
σ	Stefan-Boltzmann constant (W/m^2K^4)
τ	transmitivity coefficient

1 Introduction

This introduction serves as a means to provide with the essential aspects of this work in a compact fashion.

In the first part of this brief introduction, the tremendous effort of the European Union towards energy adequacy and environmental protection is pointed out. Hence, facts and concerns on the sustainable energy policy are presented, along with indication on the amount of electricity spent in buildings.

Heating, ventilation and air conditioning systems can consume large amounts of electricity in order to create viable and comfortable ambient conditions in buildings. Therefore, efficient methods to maintain thermal comfort are needed. A promising way to accomplish that, is to employ thermal energy storage systems.

The features of thermal energy storage are introduced in the third section. The areas in which this technology is beneficial and basic concepts of the three existing types are described briefly. Before closing this section, attention is given on the latent heat energy, which is possible using specific materials.

Finally, a discussion on computational fluid dynamics and their role in the field of fluid dynamics is conducted. Computational fluid dynamics show multiple benefits towards the theoretical and the experimental approaches and have made a big impact, mainly due to the remarkable progress in computational power over the last 20 years. Thus, it serves as a useful tool to help fulfilling the objectives of this thesis.

1.1 Electricity power production in the European Union

In the modern society the need for energy solutions is imperative. The abusive use of mineral fuels and the pollution, have led to a rapid growth in sustainable energy systems. Facts given from the International Energy Agency (IEA) [1], which is consisted of 28 country-members, are revealing; in the past decade the annual growth in wind energy exceeded 25%, while the solar photovoltaic systems rose from 1.5 gigawatts in 2000 to 67 gigawatts in the end of 2011. Moreover, the biofuels production increased up to 100 billion litres in 2010. Those facts should not strike as a surprise. Scientists and industrial partners invested in the research and development in the area of renewable energy since the decade of 1970 [2], and now the field is developing faster than ever.

The efforts have been paying off. The European Union has claimed that every country-

member has delivered its commitments for renewable energy, or even more than that, in the year 2010. Nevertheless, fears have been expressed for the future. Analysis showed that, with the current policies and obstacles, future investments may be delayed or canceled if measures are not taken [3].

A large amount of energy produced concerns electricity. It is necessary to have an overview of where this energy is consumed. Figure 1.1, in [4], illustrates the use of electricity over the years 1990-2010 in the EU-27 in units of million tons of oil equivalents. The largest amount is spent on industrial purposes, while almost 60% of the electricity produced is consumed in households or for services. It becomes evident that, a considerable large amount electricity is spent to cover energy needs in buildings.

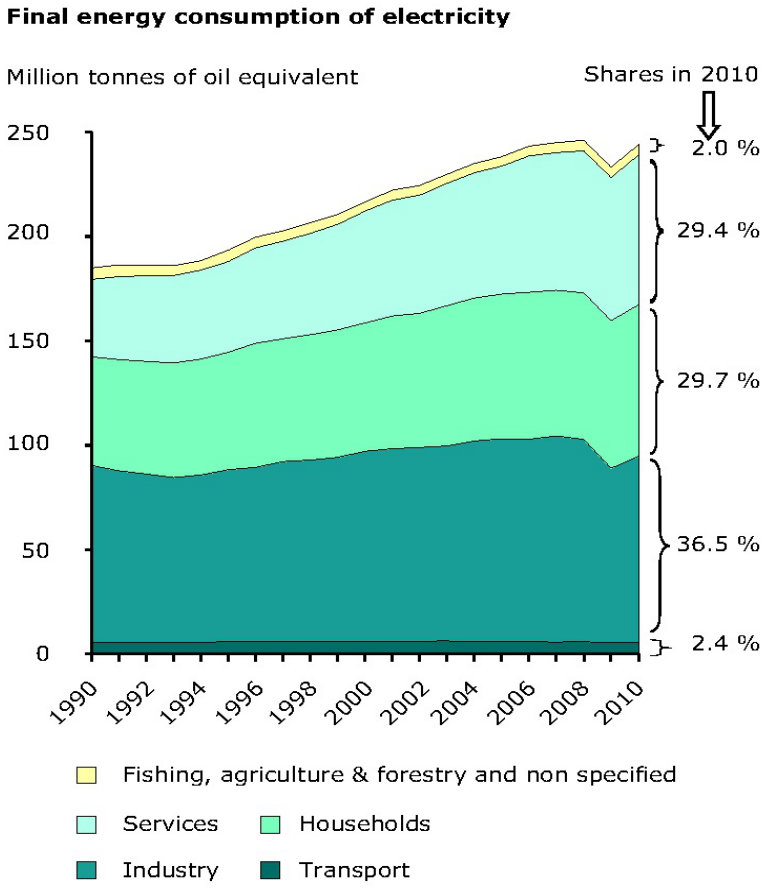

Figure 1.1 Electricity consumption in the EU-27 over the years 1990-2010 [4]

1.2 Energy Demand in Buildings

Electricity in buildings is spent, mainly, on two basic functions: lighting and thermal comfort. To achieve the latter, heating, ventilation and air conditioning (HVAC) systems are employed, in order to control and stabilize the humidity and heat load in a room.

Thermal comfort is defined by the British Standard BS EN ISO 7730 as: "that condition of mind which expresses satisfaction with the thermal environment". It is considered as one of the most important factors in the working process, as too hot or too cold environments can lead to unsafe behaviour or poor decision making. For example, workers might not wear personal protective equipment properly in hot environments, increasing the risk of injuries. Concentration is, also, affected and it can lead to serious mistakes during the execution of a given task.

Therefore, using HVAC systems is a prerequisite, to ensure safety and quality during the working procedure. However, the development of efficient systems can help towards energy savings. In that scope, passive approaches have been developed. A passive approach, in the sense that the energy source is not affected, is to utilize thermal energy storage system.

1.3 Thermal energy systems

Thermal energy storage (TES) has been a main research topic for over 30 years and can be beneficial in various occasions. TES is defined as the technology to store energy in a storage medium that can be used at a later time [5].

One of the key areas, that TES can provide solution to, is that of thermal inertia and thermal protection in buildings. In addition, implementation of TES systems in receiving systems, such as in solar energy, is very common due to the time lag between the available power and its consumption. Furthermore, extra power for security is a necessity in hospitals or large computer centres. Currently, back-up equipment is installed to provide energy in case of emergency. In that scope, TES systems can be a reliable way in the near future to minimize the costs and the size of the aforementioned applications [5].

There exist three types of TES shown in figure 1.2 [6]. The most common is the sensible heat storage. While being cheap, because storage takes place in a solid or liquid medium, such as water, this type suffers from two main drawbacks. The energy density that can be stored is quite low, and the emissive temperature during the discharge is not uniform. Issues like these can be moderated or even eliminated by incorporating phase change materials (PCM) [7, 8].

PCMs are utilized, due to their ability to go through the melting process in a specific temperature range to store latent heat energy. This is the second type of TES. The energy density that is stored during this process can be five until twenty times larger, compared to the typical sensible heat storage [6]. The difference between these two methods, regarding the amount of heat that they can store in a similar temperature range, is shown in figure 1.3 [7].

The third type of TES is the thermo-chemical storage (TCS). As molecular bonds are forming or breaking during chemical reactions, energy is stored or released. In order to exploit this feature, reversible reactions are required. The heat stored or released is affected by three parameters: the amount of storage material, the endothermic heat of reaction, and the extent of conversion [6].

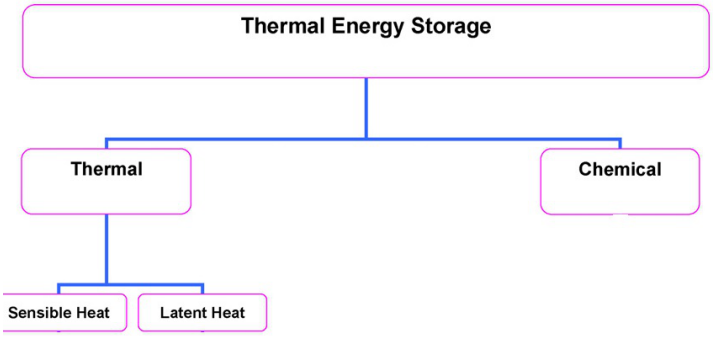

Figure 1.2 Different types of Thermal Energy Storage [6]

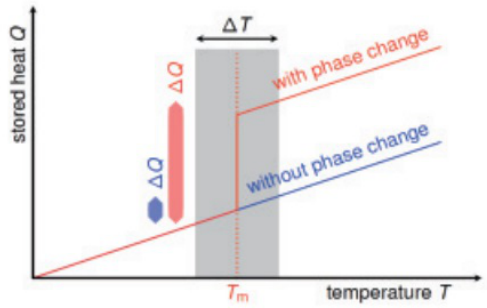

Figure 1.3 Difference in storing sensible and latent heat [7]

1.4 The role of Computational Fluid Dynamics

In the previous sections, the areas in which TES systems can be applied are shortly described. Most of them, if not all, are challenges to be addressed in the field of fluid dynamics. A solution to a problem of fluid dynamics can be obtained with theory or applied experiments or both. A relevant new approach has emerged with the ongoing development in computer power. This is called computational fluid dynamics, commonly referred to as CFD.

The physics of thermal systems will be discussed later in this work, by presenting the theory as well as mathematical equations. However, it will be made clear, that using theory is not enough to study complicated cases, at least without making significant simplifications. Here is where CFD come in handy. By applying CFD methodology, the mathematical equations are converted into algebraic expressions. The latter can be solved to obtain an amount of numbers,

which are translated into useful physical information. Furthermore, the behaviour of a specific feature can be studied under the implementation of different parameters in space and time providing with new information. In a few words: CFD can provide insight in physics.

From another point of view, a common way to investigate a complicated case is by experiment. However, experiments are limited by cost and availability of materials. Also, parameters, such us boundary conditions, or the scale of the application is restricted by nature. Some cases can prove to be dangerous as well, if chemical reactions are involved. On the other hand, these limitations do not exist with computer simulations. Therefore, various cases can be studied with a lower cost and in a wider range of parameters. In that scope, CFD can be considered as a valuable designing and optimization tool for engineers.

On the negative side, CFD are binded by the physical modeling. In example, turbulence cannot be resolved, because the physical models, also, fail to predict the behaviour of this phenomenon. In addition, solving techniques, stability issues and accuracy are still topics that continuously need to be addressed. The most significant issue, though, is the computational cost, namely the memory and the processor power.

Concluding, a phrase from J.D. Anderson, Jr. in the book [9] elucidates the role of CFD: "Today, CFD supports and complements both pure experiment and pure theory, and it is this author's [J.D. Anderson, Jr.] opinion that, from now on, it always will. CFD is not a passing fad; rather, with the advent of the high-speed digital computer, CFD will remain a third dimension in fluid dynamics, of equal stature and importance to experiment and theory. It has taken a permanent place in all aspects of fluid dynamics, from basic research to engineering design."

2 Phase Change Materials

Phase change materials are integrated in thermal energy systems to increase their efficiency, by storing latent heat additionally to the sensible heat. Therefore, an ongoing interest in these type of material is expressed over the last 10 years. A considerable amount of reviews on latent heat energy systems and phase change materials (PCM) can be found in the literature [5, 6, 10–14]. The reader can find references on desirable properties, theory, experiments and numerical approaches on the subject. Notably, PCMs are integrated not only in building applications, but also in solar energy heating, heat exchangers, automotive and others. A useful introduction in thermal energy technologies can be found in [15].

This thesis will focus on the solid-liquid phase change. The chapter begins with the basic theory on energy storage, followed by a guide on the desirable characteristics of a phase change material. These should be chosen according to the employed application.

Further on, the most common classes of materials are discussed. Organic and inorganic compounds have been tested, each presenting advantages and disadvantages. Their properties are compared, and further on their most important limitations are revealed, such as sub-cooling. In addition, the most common heat capacity measurement techniques are presented.

The chapter will conclude, with a references on characteristic experimental and numerical approaches. By studying various works, insight on the PCM applicability was gained, as well as tools to adopt to the developed computational tool.

2.1 Energy storage

The temperature of a material increases when it is heated. As long as it does not reach a critical point, where it liquifies, the temperature will keep rising. In this case the material is considered to act as a storage medium for sensible heat. The term sensible is used, because instrumentation can "sense" the temperature change. In reverse, when a liquid is cooling, before reaching the stage of solidification, it releases sensible heat. The amount of heat stored, or released, per mass is proportional to the temperature difference by a coefficient, which is called heat capacity:

$$\Delta Q = C_p \Delta T \tag{2.1}$$

, Q represents the heat energy (J), c_p the heat capacity (J/K) and T the temperature (K). This is the most common way to store heat energy in most applications.

After a critical temperature, depending on the material, the liquidation process starts. At

this point the material is still storing heat, however, temperature is almost stable. This is known as latent energy storage. The term latent is adopted, due to the fact that a thermometer cannot detect any temperature fluctuation during the melting process. This energy is utilized towards the change of the phase. Figure 2.1 [16] illustrates a typical change from the solid to the liquid phase. The latent heat is equal to the enthalpy difference, due to insignificant volume change: $\Delta Q = \Delta H$. This quantity is referred in the field of phase change materials as phase change enthalpy, melting enthalpy or heat of fusion.

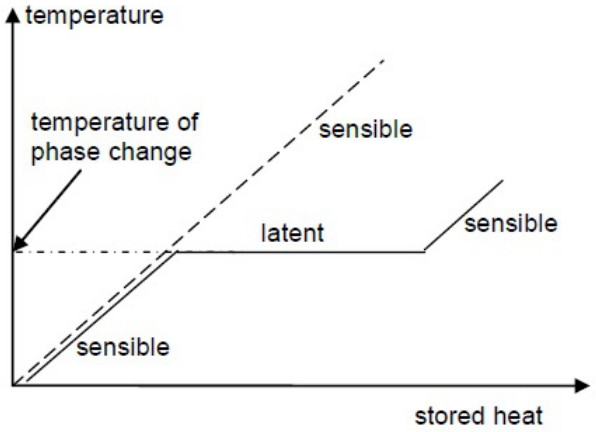

Figure 2.1 Sensible and latent energy storage as a function of temperature [15]

Phase change materials can be employed to control the temperature in a system, which is subjected in a considerable amount of heat. A typical example is keeping a drink cold by using ice. In a different perspective, keeping a room within the thermal comfort conditions can be a similar application. Another type of applications is storing heat withing a range of temperatures, in order to be used at a later time. Table 2.1 [16] shows a useful comparison, among materials which are utilized in various energy storage methods, with respect to the heat stored per volume or mass unit, and specific comments on each case.

2.2 Requirements for a phase change material

In general, a latent heat energy system should fulfill three basic constrains [6]:

i. the melting point should be appropriate for the specific application,
ii. matching heat exchange surface, and
iii. a vessel suitable to integrate the PCM.

However, successful designing demands a detailed consideration of the PCM's characteristics. They are presented as a set of requirements classified into three categories in table 2.2: physical, technical and economic, as in [16].

Table 2.1 Energy storage capability among different materials and types of storing [16]

	MJ/m^3	kJ/kg	Comments
Sensible heat			
granite	50	17	$\Delta T = 20°C$
water	84	84	$\Delta T = 20°C$
Latent heat of melting			
water	306	330	melting temperature 0 °C
paraffins	180	200	melting temperatures 5-300 °C
salt hydrates	300	200	melting tempertaures 5-130 °C
salts	600-1500	300-700	melting temperatures 300-800 °C
Latent heat of evaporation			
water	2452	120000	300 K, 1bar
Heat of chemical reaction			
H_2 gas (oxidation)	11	120000	300 K, 1 bar
H_2 gas (oxidation)	2160	120000	300 K, 200 bar
H_2 liquid (oxidation)	8400	120000	20 K, 1bar
fossil gas	32	-	300 K, 1bar
gasoline (petroleum)	33000	43200	
Electrical energy			
zinc/manganese oxide battery	-	180	
lead batery	-	70-180	

The fundamental physical property of PCM is that they can store an amount of latent energy, by changing phase, from solid to liquid and vice versa, within a specific temperature range. Hence, in each occasion, a large melting enthalpy and an appropriate operation temperature should be selected. Another crucial parameter, which is affected by the application designing, is the thermal conductivity.

Considering the effect of the temperature fluctuation on the life span and efficiency of the integrated PCM, cycling stability and sub-cooling are important. The first refers to the ability to use the material as many times as possible, from cooling to heating and back to cooling, an important feature in building applications. As a PCM can be consisted of different components, phases with different compositions can be observed; a phenomenon known as phase separation. While a PCM's temperature increases, the material does not liquify in a consistent fashion, but can show solid and liquid regions. Hence, when the solidification occurs, a different composition to the original may be formed. This phenomenon occurs in every thermal cycle in an irreversible scheme, leading to a lower heat storing efficiency. In some cases, during heating, the components can melt at the same temperature. This phenomenon is known as congruent melting.

Furthermore, in some cases lower temperature than the solidification should be reached during the cooling process. If that does not happen, then the PCM will not solidify at all. Thus, only sensible heat will be stored. This effect is known as sub-cooling (or super-cooling), shown in figure 2.3 [16]. It is desirable for the PCM to present as little sub-cooling as possible.

Regarding the use of PCM in TES, other aspects shall be taken into account. Chemical stability is necessary for a long durable product. This criterion should apply, also, within unexpected conditions, for example existence of radiation or higher temperatures than predicted. Furthermore, the compatibility with the heat transfer medium in which the latent material will be incorporated, should be addressed. Chemical decomposition and corrosion should be avoided for functioning and safety reasons, as well. Stating this, it is natural to choose a material that is non-toxic and non-flammable. Also, small volume change during the thermal cycling and low vapor pressure, minimize the mechanical requirements of the PCM's container.

Last but not least, competitive prices, high availability and ability of wide recycling of these materials have to be considered, in order to present viable solution in TES applications.

Table 2.2 Requirements of a phase change material

Physical	Technical	Economic
large melting enthalpy	chemical stability	low price
appropriate temperature range	compatibility with other materials	high availability
thermal conductivity	safety constrains	good recyclability
good cycling stability	low vapour pressure	
little sub-cooling	small volume change	

2.3 Common phase change materials - Material classes

The first, and most common material, to be used as a PCM is water, which is still considered as an excellent latent energy storage medium in cold storage applications. However, in temperatures over than 0°C different materials have to be employed. Many single components or mixtures have been tested, in order to meet the specific needs in a variety of cases [16]. In buildings, the type of phase change mostly used is that of solid to liquid and vice versa. It is handy, to illustrate these components according to the melting enthalpy and temperature, which are considered the most significant parameters. A typical example of the most promising materials is showed in figure 2.2 [15]; the figure indicates that the melting enthalpy per volume is is not exactly proportional to the melting temperature. According to Richard's theory, additional parameters to be taken into account are the number of bonds per molecule and the density divided by the molar mass [16].

Referring to building applications, the temperature range of interest is from 0 to 40°C. Within this constrain, paraffins, fatty acids,sugar alcohols, salt-hydrates and eutectic mixtures are of specific interest as shown in figure 2.2. The first three are organic materials, while the latter two inorganic.

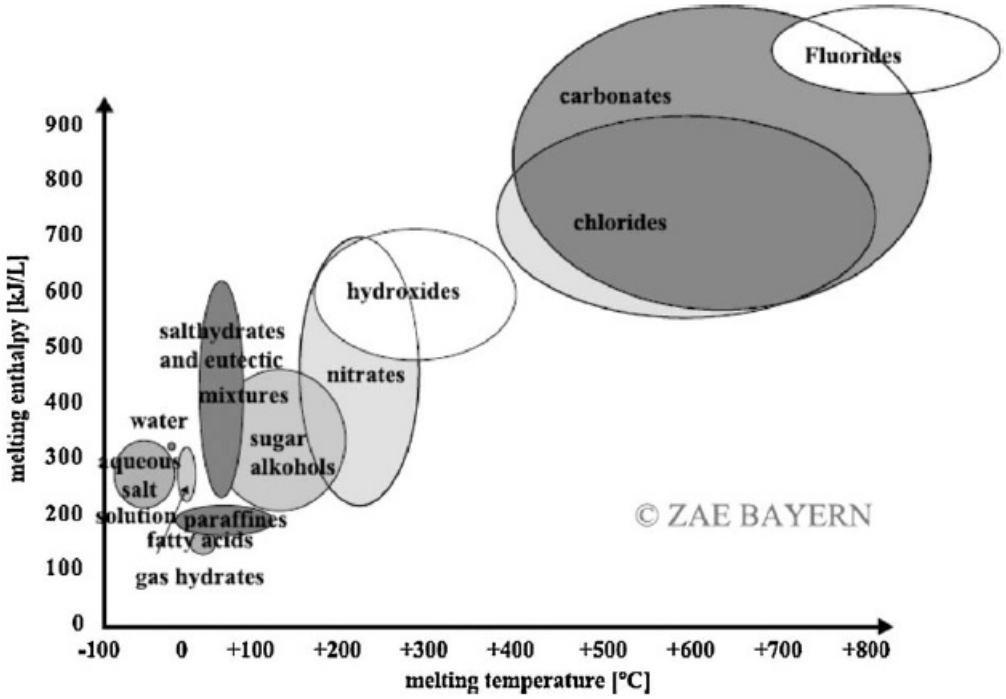

Figure 2.2 Classes of PCM materials [15]

2.3.1 Organic phase change materials

Paraffins, fatty acids, sugar alcohols and polyethylen glycol (PEG) are classified as organic materials. They are suitable for applications within a temperature range of 0 to almost 200°C. Above that, stability can be an issue. In general, compared to inorganic PCMs they suffer from a smaller density (order of $10^3 kg/m^3$), which leads to a smaller melting enthalpy per volume.

Paraffins are represented by the chemical formula: C_nH_{2n+2}. They show little or no reactivity at all with most chemical reagents. This material is considered to meet safety and containment constrains, even though the volume increases up to 10% during liquidation. Also, flammability can be an issue as far as the containment is concerned [12, 17]. Plastic containers should be avoided, due to softening. In addition, they present good storage density with respect to mass, little sub-cooling and consistent liquidation and solidification, thus good cycling stability. These characteristics have made parrafins very appealing, despite the low melting enthalpy and thermal conductivity, that they demonstrate. An interesting characteristic, is that the melting temperature increases for paraffis with increasing number of carbon atoms.

This observation has led to an interest in mixtures of different paraffins, in an attempt to create PCMs with wider temperature range.

Further on, the chemical formula of fatty acids is: $CH_3(CH_2)_{2n}COOH$. In general, their characteristic match to those of paraffins. Their cycling stability is certain, because they consist only of one component, thus phase separation is not observed. As in the case of paraffins, different fatty acids can be mixed to produce a PCM which operates in a wider temperature range compared to the single case.

A relatively new material in this class is sugar alcohols. With chemical formula $HOCH_2[CH(OH)]_nCH_2OH$ they are used in a temperature region above 90 and below 200°C. They show high density and melting enthalpy density compared to the other organic PCM, but also some sub-cooling. As it is a new material, there is not enough information about it yet, except the fact that they very safe.

Polyethylen glycol (PEG) is a polymer described by the chemical formula: $C_{2n}H_{4n+2}O_{n+1}$ and has a base unit of monomers -CH_2-CH_2-O- . Depending on their molar mass they demonstrate a rather small temperature limits, but are investigated as a cost effective shape-stabilized phase change materials [18].

2.3.2 Inorganic phase change materials

Salt hydrates and eutectic mixtures are inorganic materials. A mixture of salt and water is the composition of this materials. Water molecules are assigned to each ion pair of the salt and are oriented in a distinctive fashion. A stable crystal structure is formed, due to the ion-dipole or hydrogen bonds. They are employed in cases where temperature ranges between 0 to almost 150°C, although different salts can be used for higher temperatures. A variety of compounds that can be used as salts can be found in [5, 11, 15, 16].

A favourable characteristic is that they present a large density of $1g/cm^3$, which leads to a higher volumetric melting enthalpy than organic materials. In addition thermal conductivity is comparably bigger. On the other hand, compatibility with metals can be limited, as in some occasions corrosion has been observed [15]. However, due to the presence of different components sub-cooling is a considerable drawback. In addition, most salt hydrates melt incongruent. This process leads to a consecutive decrease in the efficiency in the energy storage.

Combining two or more ingredients can lead to eutectic mixtures. In this case, these two ingredients solidify at the same instant out of the liquid at a minimum freezing point, also called eutectic point. However, the presence of two different solid phase does not lead to phase

separation, as the overall composition is still the same as in the liquid. Usually, a inhomogeneous melting is observed, although it is not a strict rule in cases where sub-cooling is observed in the lower salt hydrate, making the process irreversible and leading to the continuous decline in their storage efficiency. Highlights on the theory of phase separation can be found in [16].

Having described the most significant features of PCM, a comparison of the advantages and drawbacks of organic and inorganic materials, is illustrated in table 2.3. In any case, no specific type is superior to the other. Furthermore, in order to apply the most suitable, a study on the climatic conditions and the favorable situation should be first conducted [19].

Table 2.3 Advantages and disadvantages of organic and inorganic PCM

	Organic	Inorganic
Advantages	low/no sub-cooling no corrosion stability (chemical and thermal)	greater melting enthalpy lower cost
Disadvantages	lower melting enthalpy low thermal conductivity	sub-cooling corrosion phase separation congruent melting (unstable efficiency)

Examples of both organic and inorganic PCMs and their properties can be found in [16] and more extensive guides, which include commercial materials, are given in [5, 11]

2.4 Inherent limitations

In the previous sections, issues that are connected to the nature of the materials have been discussed. Sub-cooling, phase separation, low thermal conductivity and containment are the most important issues to be addressed.

2.4.1 Sub-cooling

Sub-cooling can be present in both organic and inorganic materials and as already mentioned, the solidification temperature may be lower than the melting, figure 2.3. The reason behind this effect lies in the solidification process. Initially, only a small solid particle, the nucleus, is starting to grow at the boundary of the interface between the liquid and the solid phase. Surface energy (proportional to the surface area - r^2) and heat released by the phase change (proportional to the volume - r^3) set an energetic prerequisite; that the particle has to be of a sufficient large radius for the solidification to be initiated. This can cause a significant problem, when heat release is important for temperature stability applications, in example

maintaining a warm interior, as in some cases lower temperatures have to be reached to before the solidification can start.

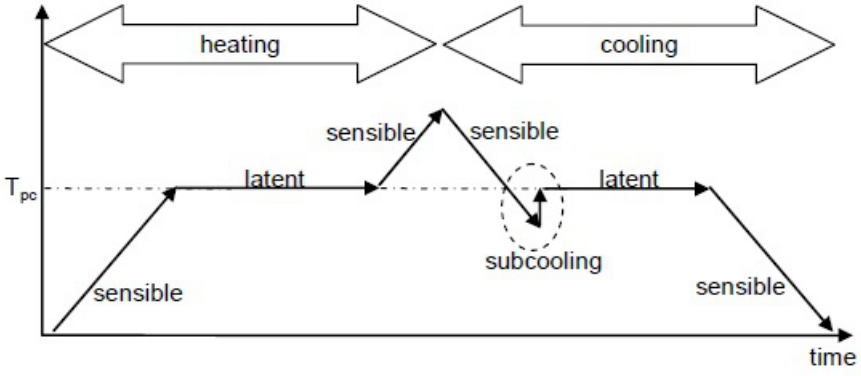

Figure 2.3 Temperature change during heating and cooling of a PCM with sub-cooling [16]

To counter this problem, special additives, also called nucleators, can be included in the PCM's composition. They help to reduce the sub-cooling to a few degrees. However, it is not straightforward to develop such a component, as the underlying mechanism is not completely known. Therefore, nucleators have been employed with the most well-investigated PCMs [16].

A different approach, is to enforce a low temperature in a single position. This method can be applied with a Peltier element or the cold finger technique. Locally, a cold region is employed, which assists the solidification. However the melting temperature should be higher than the ambient. Recent research is taking advantage of the fact that high pressure can lead to nucleation. However, there is still need for more investigation on the matter [16].

2.4.2 Phase separation

Phase separation is another important issue, which severely affects the energy storage efficiency of salt-hydrates. During this phenomenon, the components of the PCM can be found in different phases.

To counter this problem, artificial mixing is used with success in many cases of salt-hydrated PCMs. However, this method does not depend on the main material and special equipment is necessary. A more convenient way to deal with this problem, is to increase the content in water. However, heat storage decreases and the melting range increases. A more suitable solution lies in the concept that the salt hydrate can be held together. Two ways to accomplish are gelling or thickening. In the first method, a network that holds the salt hydrate together is established in three dimensions. In thickening, the viscosity of the material is increased, thus, different phases cannot separate far until the material is solid. The best solution, although it

is difficult to employ, is by achieving congruent melting, as the material can then be used in any condition [16].

2.4.3 Low thermal conductivity

A factor that has a negative impact on the heat transfer is the low thermal conductivity of the PCM. To improve heat transfer two ways are available; convection in the liquid phase, or adding objects (small particles) with larger thermal conductivity, in the PCM left figure 2.4 [15]. Also, adding metal fins to the heat exchanger is another approach, right figure 2.4. In each case, the thermal conductivity can be increased with suitable encapsulation [16].

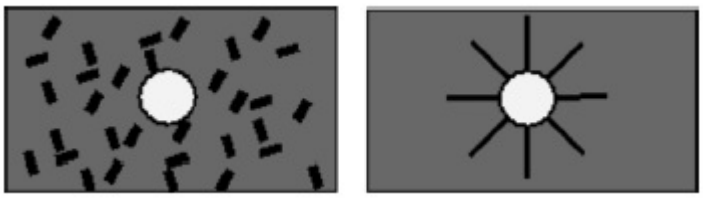

Figure 2.4 Methods to improve thermal conductivity within the PCM [15]

2.4.4 Containment and material compatibility

In early applications the PCM is directly impregnated to a porous material, such as concrete, gypsum and others. However, serious leakage is reported in many cases, thus this method is considered to be unreliable, because the PCM should be kept in the assigned position at all times. In addition, a leakage can be harmful for the environment or it may affect the efficiency of the PCM. For these reasons, a vessel is used to store the PCM. This procedure is called encapsulation. Preventing leakage is not the only advantage of encapsulation; thermal conductivity can, also, be improved, while it contributes to the mechanical stability in cases that the PCM is a building element [12]. There are two types of encapsulation, regarding the size of the vessel; macro- for several milliliters or larger, and micro- for smaller scales, in example particles of 1 to 1000 μm.

Macro-encapsulation is observed in most cases. The containers, which are available in a wide variety, can be made from plastic or metal. Their main utilities include leakage prevention and improvement of thermal conductivity, but they also make the PCM incorporation easier to handle. The geometry of the encapsulation may affect the efficiency of the heat transfer, as the most important dimension is thickness. Among the available options, which are balls (spherical geometry), pipes (cylinders) and slabs (plates), the best option is the slab, due to the small

thickness to length ratio [16].

Micro-encapsulation is a newer method. The aspects are similar, but due to the very small sizes, the surface to volume ratios is very large. This leads to a further improvement on the thermal conductivity. In addition, the phase separation is observed in microscopic distances. Subsequently, an enhanced cycling stability of the PCM occurs. However, the container material should be carefully chosen, in order to prevent chemical reactions. Geometry is not an important parameter as the container's dimensions are negligible to the whole application.

An additional key issue is the combination of PCM with other materials, whose concentration are very small compared to the PCM. This process leads to the production of composite materials, with even more enhanced characteristics [15].

In this point, the importance of ensuring the compatibility of the PCM to the container material, for operating and safety reasons, is highlighted. The most common problems, that should be tackled before any PCM application is employed, are listed below:

- corrosion of metals in containers by inorganic PCM
- softening of plastic in containers by organic PCM
- infection of the PCM structure from the container's material in liquid or air transfer.

2.5 Measurement of the thermal properties of phase change materials

In order to properly design and assess a latent heat energy system, the thermal properties of the PCM have to be determined. The two most important properties are the reproducible phase change and the stored heat capacity. To test the cycling stability, a sample of PCM is subjected to continuous heating and cooling up to 15°C around its melting temperature, ensuring that the PCM has indeed melted each time.

To obtain the heat capacity two methods are most commonly used: the Differential Scanning Calorimetry (DSC) and the T-history. The basic concept is to provide or extract an amount of heat ΔQ, with a calorimeter, and measure the temperature change ΔT. After that, using equation 3.2 the specific heat c_p can be calculated. Three properties are involved in this procedure; the melting point, the melting enthalpy and the specific heat. Keeping in mind that a PCM has a range of melting temperature the first two properties can not be exactly defined. Therefore, the amount of heat should be supplied in temperature intervals.

In DSC two samples are used; on one side a material, the specific heat of which is well defined and on the other the PCM of interest. The procedure is as follows: supplying heating

power to the two samples in different chambers, they are heated, while forced being at the same temperature at each instant. The difference in power supply is used to extract the unknown specific heat capacity (c_p), which is the heat capacity per unit mass and has units J/kgK. Another, possible setup is to keep the two samples in the same chamber, provide heat to raise the ambient temperature, and measure the difference in the heat flow rate between the two materials. In any case, when using this technique some aspects should be highlighted:

i the weight of the samples is very small, only a few grams, thus the information provided consider the local properties and the sampling process has to be handled with extra care,

ii the measured curves are not the physical ones, as physical phenomena such as the thermal inertia, the convection in the sample and the heterogeneous temperature of the PCM and the container's vessel are not included in the consideration, and

iii the temperature intervals have to be very small (order of 0.5°C/min).

In the T-history method, an experiment among PCM samples (two or more) and a well known material during the cooling process is conducted. First, all materials are placed in tubes in liquid phase. Suddenly, a well controlled environment is set upon them, forcing them to cool down. As the time passes, the materials experience liquid cooling, solidification and solid cooling. In the end, a temperature curve is obtained for each material. Comparing the temperature curves of the well known material to the PCMs, the heat capacity, the melting point and the melting enthalpy of each one, can be mathematically obtained [15]. This procedure is suitable for larger samples, more economic and allows optical observation of the solidification phenomenon compared to the DSC method.

2.6 Phase change materials on the market

Leading companies in commercial production of PCM are:

- RUBITHERM GmbH in Germany
- Dörken GmbH & Co. KG in Germany
- Climator AB in Sweden
- TEAP in Australia
- CRISTOPIA Energy Systems in France
- Mitsubishi Chemical in Japan

. The prices can be varied from 0.5 to 10 € per kilogram [15].

2.7 Literature Review

The underlying physics governing the phenomenon of phase change can be approached by crystallization kinetics and multi-component thermodynamics. However, theoretical studies close to the melting temperature on this field are rare, due to the volatile behaviour of phase change materials. Hence, experimental and computational studies are required in order to enhance the physical insight and successful implementation of PCMs in real applications. It is out of the scope of this work to present nucleation theory, but the reader can find useful information in [16, 20].

2.7.1 Experimental studies

In a review conducted by Kuznik [12], it is reported that, more than 60% of the published studies present experimental work, with half of them specialized on walls with PCM. The specific paper provides useful literature of various sources on the subject.

Various studies were carried out in order to compare the thermal behaviour of the same application, with and without integrated PCM [21–32]. In all these papers, the outcome verifies the beneficial effect of the former in thermal control, within a variety of conditions. In addition, the behaviour of two and four different combination of wallboards with PCM were compared in [33] and [34] respectively, whereas the efficiency of blinds is evaluated both in laboratory and real conditions in a work of Weinlaeder et. al. [35].

In addition to application assessments, experiments are conducted in order to determine the properties of the PCM, such as the heat capacity, melting temperature, volume contraction and others, in a range of conditions [36–41]. An interesting study which utilize both experimental and computational techniques to investigate heat storage and release can be found in [42]

An additional aim of the literature research was, to find a suitable experimental case to be used as a validation case for the developed numerical method. In order to accomplish that, input and output data should be clearly presented and evaluated. Also, the initial and boundary conditions should be clearly stated. It is obvious that in any occasion, the building application should be described in detail and incorporate a PCM material, which properties we could obtain from the literature.

Although results obtained form experimental works in ambient conditions are full of valuable conclusions [21–26, 30, 32], it is not convenient to reproduce their initial and boundary conditions for computational reasons. Usually, those conditions are not described extensively, and even when they do, the incorporation is quite challenging especially for the air velocity field.

Hence, only the studies that were conducted in a controlled environment (climatic chamber or laboratory) [27–31, 34, 35] were considered as validation cases.

One of Kuznik's work [28], where a cube situated in a climatic chamber is subjected to a sinusoidal thermal fluctuation, provides all the necessary data to proceed to a numerical validation. However, difficulties were experienced during the transient simulation of the air inside the cube. A possible explanation could be a pressure build up, as no mass exchange is taking place between the fluid inside and outside of the testing cube. Therefore, a more suitable case was considered to be the assessment of the blinds containing PCM in [35], with the assumption of an air inlet and outlet far from the blind. Also, this case provides with insight on thermal radiation implementation.

2.7.2 Computational studies

Computational methods have been employed as a means of investigation of the PCM's capabilities in various applications. To validate, use or improve those numerical tools experimental data are often required [21, 26–28, 31, 33, 43–45]. Various computational schemes, such as finite differences, volumes and elements, have been used in the development of in-house codes or in commercial packages. One dimensional simulations have been carried out to provide physical insight or predict characteristics in various cases [21,33,43,44,46,47]. Comparison to the experimental results are often quite good, giving motivation for further improvement of the numerical methods. In all these works, the modeling of the energy stored and released is specially treated and is the most important feature in the simulation procedure.

The heat flow curve can be represented by a user defined function, where temperature is the independent variable, and can be quite accurate to the DSC curve for a specific PCM. In Neeper's work [48] the specific heat capacity was modeled by the expression:

$$c_p = A + \frac{B}{W} exp\left[-\left(\frac{T - T_m}{W} \right)^2 \right], \tag{2.2}$$

where A is the amount of sensible heat, and the total latent heat capacity is the integral of the exponential term equals to $B\pi^{1/2}$, T is the room temperature and T_m is the melting temperature. The term W represents the temperature difference in which 84% of the latent capacity occurs, in other words the half-width transitions, which was set to 0.5 and 2.0 for comparison reasons. A useful conclusion of this work was, that the efficiency of energy storing is related closely to the temperature cycle.

More recent, Evola et. al. [19], evaluated a PCM honeycomb wallboard, using four indica-

tors; the intensity of thermal discomfort, the frequency of thermal comfort, the frequency of the PCM's activation and the efficiency of the PCM (η_{PCM}). The curve of the specific heat and the indoor temperature have a great impact on the suitability of the selected PCM and is expressed as:

$$c_p = \begin{cases} 1200 + 18,800exp\left(-\frac{T_p - T}{1.5}\right) & ,T < T_p \\ 1300 + 18,700exp\left(-4(T_p - T)^2\right) & ,T \geq T_p, \end{cases} \tag{2.3}$$

where T_p is the peak temperature. Clearly the first term on the right hand side represents a sensible heat and the second the the latent heat capacity. Similar expressions can be found in [27, 28]. In these studies, different curves are used for the heating and cooling process, due to the hysteresis observed in the DSC curves.

In [45], this function is a polynomial up to the third order of temperature. A similar procedure is used in [33]; the enthalpy (h) and temperature are calculated in each timestep from a user defined function and therefore the correct specific heat capacity is obtained in each node (i) as : $c_{p,i} = \frac{h_{i,new} - h_{i,old}}{T_{i,new} - T_{i,old}}$. Instead of temperature, the air velocity at the exterior side of the wall can be used as the independent variable as in [46].

However, every material is characterized by a different DSC curve, which is not always possible to obtain. A different approach is that of the effective heat capacity method [49, 50]. The melting enthalpy (L), the melting (T_m) and solidification (T_s) temperatures are combined in a simple formula:

$$c_p = \frac{L}{T_s - T_m} + c_{pl}, \tag{2.4}$$

where c_{pl} is the specific heat of the liquid PCM. A similar procedure is found in [21,26,31,43,44]. This method is more general and is adopted in the numerical method. Excelent results have been reported using this method in [44]. An example is showed in figure 2.5 [15], where the real curve of the heat capacity coefficient is plotted with the dashed line and the effective with the dotted line.

It should, also, be mentioned that the space and time scale should be taken into account regarding building applications. The energy needs for the whole building throughout a year's time should be evaluated, to serve designing purposes. Hence, it is clear that computational cost is a constraining factor for the methods described above. A promising approach of modeling the PCM with constant resistant and capacitors (RC) is described in [51].

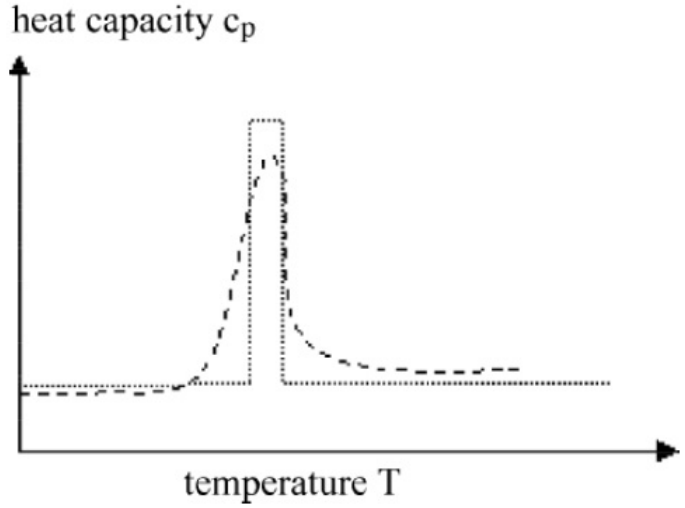

Figure 2.5 Real (dashed-line) and effective (dotted-line) heat capacity [15]

3 Underlying Physics and Numerical Modeling

The purpose of this thesis is to investigate the way a PCM can have a positive impact on thermal comfort. This case is considered complex, due to the fact that various physical phenomena take place. Energy transfer due to an external heating source causes fluctuations to the temperature and flow field of the investigated domains. Therefore it is important to clarify thermodynamic concepts. A short discussion on topics such as thermodynamic system, variables and forms of energy, opens this chapter.

The second part is dedicated to heat transfer. Although, every type of heat transfer is covered, the mechanisms of natural convection, radiation and heat transfer through multi-layer bodies are of special interest within this work. Therefore, an extensive description on these topics is necessary.

The Navier-Stokes equations are presented in the following part. They are used to describe the flow in any given domain, assuming that the continuity is satisfied. They consist of partial differential equations in space and time, which express the three principles governing any physical phenomenon: the mass conservation, the second Newton's law and the conservation of energy.

Finally, the basic concepts of the finite volume computational method are described. This method is used to simulate the cases studied in the next chapter. A quick introduction in topics, such as grid generation and the implementation of boundary conditions concludes this chapter.

3.1 Thermodynamics

The definition of the term thermodynamics can be stated as the science of moving force heat [52]. The second thermodynamic law states that energy flows from a warm system to a cold, due to the temperature difference. Thermodynamics are connected closely to heat transfer, which describes the way of this energy transfer and allows the specification of the temperature distribution as a function of space and time [53]. Therefore, one can claim that the role of thermodynamics is to state laws and principles that govern thermal phenomena, while the properties which characterize them can be calculated with tools and equations (mechanisms) provided by heat transfer. Combing those two sciences is essential, towards the fulfillment of the main purpose of a thermodynamic assessment; that is to identify the macroscopic state and the occurring changes in the case being studied.

3.1.1 Types of systems

To begin with, every process and property in an analysis refers to a predefined system. A system can be classified as one of the following types; open, closed and isolated, figure 3.1 [52]. An open system is able to exchange energy and mass with its surroundings through its boundaries, whereas a closed one can exchange only energy. In the latter type every kind of transfer is blocked, in example a room with adiabatic walls and no openings.

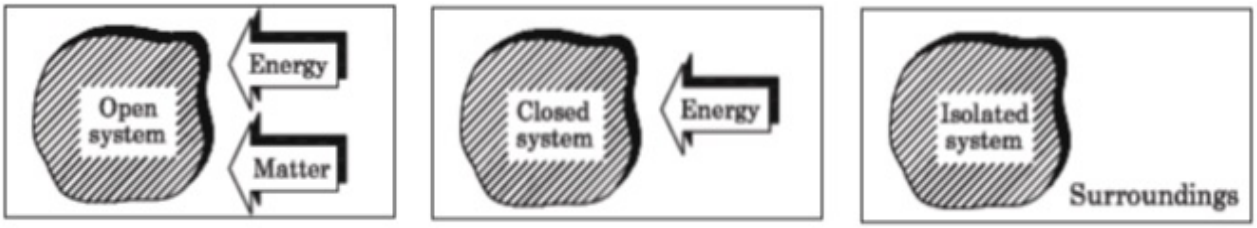

Figure 3.1 Types of systems in thermal analysis [52]

3.1.2 Variables

The results of the assessment are translated into physical quantities which describe the system. Thus, defining a number of quantities as variables is a part of the analysis. The variables of a system depend on each other, following specific laws, such as the ideal gas law or the Navier- Stokes equation, and can be intensive or extensive. Intensive variables have values, which do not depend on the size of the system, such as temperature. Extensive, on the other hand, depend on the volume of the system. It should be noted that a variable can be intensive or extensive, so as explicit details should be given; heat capacity (C_p), with units J/K, is an extensive variable but one can refer to the heat capacity per mass, known as specific heat capacity (c_p) with units J/kg K, in order to describe the intensive parameter. Extensive variables are usually denoted with capital letters, whereas intensive are represented with the lowercase.

In this point a number of important variables should be mentioned, revealing the complexity a system can have; entropy, enthalpy, internal energy, heat energy, work, pressure, temperature, volume, mass, density, heat capacity (at specific pressure or volume), and so on. Fortunately, it is at the discretion of the researcher to choose which of those to use, to describe and evaluate a specific work.

3.1.3 Energy

It has been already mentioned that a lot of research material is produced every year in the scope of serving energy needs. Energy is measured using the quantities work and heat. These quantities are positive if energy is introduced into the system and negative if energy is extracted.

Work (W)

The concept (and quantity) of work is used when the energy exchange process takes place as an organised action. In general work is defined as the action of a force by a unit of distance and has units of Joule (J). Assuming a generalized force F_i and a generalized displacement X_i, the total work W is the sum of all the individual products:

$$W = \sum_i F_i X_i \tag{3.1}$$

Significant forms of work in physics are considered the following :

i. the mechanical work,
ii. the volume work,
iii. the surface work, and
iv. the electrical work.

Heat (Q)

Energy exchange can occur in an uncoordinated way, pointing out to the random impacts between particles. In that case, energy is transferred from the high-energy particles to the low-energy particles; temperature difference is the reason and the phenomenon is described as heat transfer having also units of Joule (J). Heat capacity is the link between the two aforementioned quantities and is a property of the substance present in the system. The definition is:

$$c_p = \frac{\Delta Q}{\Delta T}, \tag{3.2}$$

stating that the increase (or decrease) of heat is proportional to the temperature difference by the value of the heat capacity. Heat capacity is an extensive variable and has units (J/K). Referring to general cases, and when listed in tables, it is convenient to insert an intensive variable which represent the heat capacity; the specific heat capacity: $c_p = \frac{1}{m}\frac{\Delta Q}{\Delta T}$,with units (J/ kg K). It is, also, known that in the thermodynamic processes, pressure and volume also

varies with the temperature when heating or cooling a system. Depending on whether pressure or volume is kept stable, the heat capacity can be calculated with different values leading to c_p or c_v. Regarding liquids and solids the difference between them is negligible. For gases c_p is larger than c_v, fact that is justified because part of the energy is being spent to volume work.

3.2 Heat Transfer

The main aspects of the three mechanisms of heat transfer are presented next: conduction, convection and thermal radiation. Conduction is observed among all motionless objects, whereas in convection a fluid flow is required. Thermal radiation occurs between two objects even when they are in vacuum conditions; in fact in vacuum the phenomenon is more intense. Finally, a discussion on overall heat transfer closes the present section.

3.2.1 Conduction

To describe the energy flow the term of heat flux ($\dot{\mathbf{q}}(x,t)$) is introduced. The magnitude and the direction of the energy flow, in space and time, is represented by the vector field of heat flux. Heat flow is obtained through the heat flux through a surface element:

$$d\dot{Q} = \dot{\mathbf{q}}(x,t)\mathbf{n}dA = |\dot{\mathbf{q}}|\cos\theta dA, \tag{3.3}$$

where $\dot{Q}$ represents the heat flow, $\mathbf{n}$ is the unit vector normal to the surface pointing to the outer direction, A is the surface and θ the angle between the heat flux and the normal vector. The heat flow has units (J/s) or (W), while the heat flux J/s m^2 or W/m^2.

In heat conduction, the most distinctive characteristic is that the energy is transferred among motionless objects, which can be in the gaseous, liquid or solid phase. Two mechanisms incite this feature: the first one results from the interaction among the molecules. High energy molecules, due to Brownian motion, spinning and oscillations, are transferring energy to molecules with lower energy. This energy difference is observed macroscopically by the temperature gradient. The second is due to the diffusion of the free electrons that are present in metals. That explains the fact that metals are in practice better thermal conductors than other media. Conductivity (k) is a property of the material and a very important factor of the heat that will flow through the surface of the body. It is defined by the magnitude of heat flux over the temperature difference in the specific direction, and has units (W/mK). For example, in

Cartesian coordinates on the x-axis the conductivity is:

$$k_x = -\frac{q_x}{\partial T/\partial x}, \tag{3.4}$$

the negative sign is present, because flow occurs from the higher to the lower temperature. The conductivity is affected by the properties and the internal structure of the material and can be a function of temperature and pressure. A more uniform co-ordinance of the molecules in a crystalline structure leads to a higher the thermal conductivity, while an irregular structure has the opposite impact. The capability of insulators to present a very low conductivity is justified by their porous-like construction, because air, a very efficient insulator, is trapped inside the pores. With decreasing thermal conductivity the various materials can be sorted as follows: clear metals, metal alloys, liquid metals, non-metallic solids and liquids, solid insulators and gasses [53].

The heat flow can be calculated by the Fourier law, expressed in the Cartesian coordinate system as follows:

$$Q_x = -k_x A_x \frac{\partial T}{\partial x}, \quad Q_y = -k_y A_y \frac{\partial T}{\partial y}, \quad Q_z = -k_x A_z \frac{\partial T}{\partial z}, \tag{3.5}$$

where A is the surface of each side (m^2).

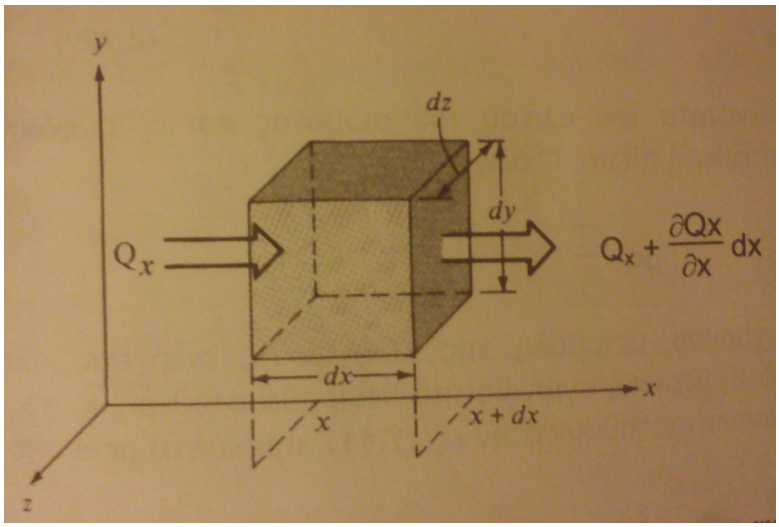

Figure 3.2 Three dimensional conduction in a cubic element [53]

The original objective is to calculate the energy distribution in space and time. By dictating

the energy flow on a cubic element, shown in figure 3.2 [53], a differential equation is derived:

$$Q_x + Q_y + Q_z + \Phi dxdydz = \left(Q_x + \frac{\partial Q_x}{\partial x}dx\right) + \left(Q_y + \frac{\partial Q_y}{\partial y}dy\right) + \left(Q_z + \frac{\partial Q_z}{\partial x}dz\right) + \rho c_p \frac{\partial T}{\partial t}dxdydz, \tag{3.6}$$

where Φ represents the heat sources at the element. If the heat flow is substituted from equation 3.5, and assume that the thermal conductivity is equal in every direction, that is $k = k_x = k_y = k_z$, then the following equation is derived:

$$k\left[\frac{\partial^2 T}{\partial x^2} + \frac{\partial^2 T}{\partial y^2} + \frac{\partial^2 T}{\partial z^2}\right] + \Phi = \rho c_p \frac{\partial T}{\partial t}, \tag{3.7}$$

which is the equation for non-steady heat transfer with conduction in Cartesian coordinates. Note that $\rho c_p \frac{\partial T}{\partial t}$ is the change of the internal energy of the body in the unit of time.

Three distinctive cases exist, which can lead to well known equations:

1. if there are no heat sources then $\Phi = 0$ and equation 3.7 becomes:

$$k\left[\frac{\partial^2 T}{\partial x^2} + \frac{\partial^2 T}{\partial y^2} + \frac{\partial^2 T}{\partial z^2}\right] = \frac{\rho c_p}{k}\frac{\partial T}{\partial t}, \tag{3.8}$$

   which is known as Fourier equation,

2. if the conditions are steady the derivative of time is zero, leading to:

$$k\left[\frac{\partial^2 T}{\partial x^2} + \frac{\partial^2 T}{\partial y^2} + \frac{\partial^2 T}{\partial z^2}\right] + \frac{\Phi}{k} = 0, \tag{3.9}$$

   known as the Poisson equation, and

3. by combining the two previous conditions we derive a Laplace equation:

$$k\left[\frac{\partial^2 T}{\partial x^2} + \frac{\partial^2 T}{\partial y^2} + \frac{\partial^2 T}{\partial z^2}\right] = 0 \tag{3.10}$$

Note, also, in the first case the ratio $\frac{k}{\rho c_p} = \alpha$ is known as the thermal diffusivity.

3.2.2 Convection

In contrast to conduction, convection is observed in case of a flowing media (liquid or gas) on a solid surface, with temperature difference between them. The macroscopic movement

leads to an additional enthalpy and kinetic energy to the heat transfer, superposing the effect of conduction. Close to the contact region of the fluid with the solid surface, two layers are developed: i) the hydrodynamic boundary layer (δ_T) due to the velocity and ii) the thermal boundary layer (δ_T) due to the temperature difference.

To calculate the heat transfer, a heat transfer coefficient (h), with units (W/m^2), is introduced and is defined as the ratio of heat flux at the surface of the wall over the temperature difference of the wall and the core of the fluid:

$$h = \frac{\dot{q_w}}{T_w - T_f} \tag{3.11}$$

However, both the coefficient and the heat flux are unknown. An approach to calculate the latter is to make use of the conduction very close to the wall, where the velocity of the fluid is zero, assuming the no-slip boundary condition. Hence, on the wall the heat flux is:

$$\dot{q_w} = -k \left(\frac{\partial T}{\partial y} \right)_w , \tag{3.12}$$

assuming the x-direction along the wall and y- normal to the wall. This leads to:

$$h = -k \frac{\left(\frac{\partial T}{\partial y} \right)_w}{T_w - T_f} \tag{3.13}$$

Equation 3.13 shows that, a small ratio k/h denotes a good heat transfer, while a large one shows low heat transfer capability. This interesting fact is linked to the hydrodynamic boundary layer: the thicker it becomes, the more difficult it is for the heat to be transferred. It becomes obvious that, the temperature field is affected by the velocity field. Thus, physical model should combine thermodynamics and fluid mechanics to capture the thermal and flow characteristics.

It is important to note that, the heat flux and the associated heat transfer coefficient are local variables. It is more useful, to obtain a mean heat transfer coefficient by integrating the local heat transfer coefficients over a surface of interest:

$$h_m = \int_A h dA \tag{3.14}$$

For simple cases, such as fully developed laminar flows in tubes or flow over a parallel plate, the approach described above is handy. However, the calculation of the heat transfer coefficient is a

difficult task to be treated by theoretical consideration alone in more general cases, by solving the differential equations for temperature and velocity.

Therefore, experimental methods are, commonly, used to determine the heat transfer coefficient, by calculating the heat flux and the temperature on the wall and the fluid. We have described such methods in chapter 2. By using equation 3.13, the heat transfer can be extracted. It is useful to apply the similarity theory, in order to match different experimental data. The relative parameters, typically numbered between 5 and 10, are grouped into dimensionless numbers. The most appropriate in these cases are the Reynolds, Prandtl and the Nusselt number:

$$Re = \frac{\rho u_0 L_0}{\mu}, \tag{3.15}$$

is the ratio of the inertial to viscous forces,

$$Pr = \frac{\nu}{\alpha} = \frac{c_p \mu}{k}, \tag{3.16}$$

is the ratio of the viscous diffusion rate to the thermal diffusion rate, and

$$Nu_x = \frac{hL_0}{k}, \tag{3.17}$$

is the ratio of the convective heat transfer to the conductive heat transfer. The index x indicates a specific position on the surface. Typically empirical relationships have been extracted among these numbers for a range of cases: turbulent flows, flow normal to cylindrical or non-cylindrical spherical objects, bundle of tubes and others. These relationships are of the form:

$$Nu_x = f(x, Re_x, Pr) \tag{3.18}$$

The similarity theory and the dimensionless numbers are, also, useful in the development of numerical schemes, besides serving as a useful tool to compare data among a large number of simulations.

Finally, depending on the applicable forces on the flow, convection is categorized into forced and natural convection. When the flow is created by a pump or a compressor, the convection observed is called forced. The boundary layer developed is not restricted from neighboring surfaces, while in the core of the flow (a region distanced enough not to be effected by the wall presence) the temperature and velocity fluctuations are negligible.

Natural Convection

It is well known that, the density of a fluid depends on the temperature. Therefore, temperature differences lead to density gradients. Combining the buoyancy, which states that the lighter fluid will rise and the heavier will descend, a flow is created. The convection in this case is called natural. The velocities characterizing this phenomenon are quite small comparing to the forced convection, so the Reynolds number is not appropriate to characterize the flow.

To study this kind of flow, first, the conservation equations are presented, in two dimensions using the Cartesian coordinate system as in figure 3.3:

- Mass conservation:

$$\frac{\partial u}{\partial x} + \frac{\partial v}{\partial y} = 0 \tag{3.19}$$

- Momentum conservation:

$$\rho \left(u\frac{\partial u}{\partial x} + v\frac{\partial u}{\partial y} \right) = -\rho g - \frac{\partial p}{\partial x} + \mu \frac{\partial^2 u}{\partial y^2} \tag{3.20}$$

- Energy conservation:

$$\rho c_p \left(u\frac{\partial T}{\partial x} + v\frac{\partial T}{\partial y} \right) = k\frac{\partial^2 T}{\partial y^2} \tag{3.21}$$

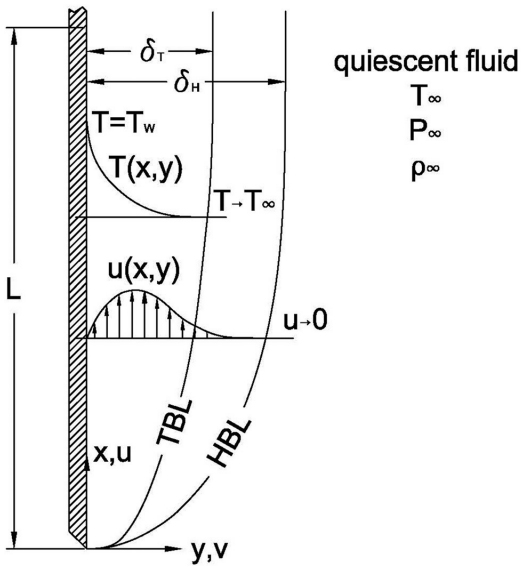

Figure 3.3 Natural convection in two dimensions [54]

Equation 3.20 is studied. The first term on the right hand side, expresses the gravity force in the x-axis, as shown in figure 3.3 [54]. The second term stands for the pressure gradient on

the same axis. In a region where the fluid is quiescent (u→0) and the density is considered steady ($\rho \to \rho_\infty$), this term is calculated as:

$$\frac{\partial p}{\partial x} = -\rho_\infty g, \tag{3.22}$$

and with some algebraic manipulation we derive:

$$-\rho g - \frac{\partial p}{\partial x} = (\rho_\infty - \rho)\, g \tag{3.23}$$

The density change, due to the temperature difference under steady pressure, can be expressed as:

$$\beta = -\frac{1}{\rho}\frac{\partial \rho}{\partial T}, \tag{3.24}$$

where β is defined as the volumetric temperature expansion coefficient. An equivalent form is:

$$\rho_\infty - \rho = -\beta\rho\,(T_\infty - T)\,, \tag{3.25}$$

where T_∞ is the temperature in the quiescent fluid. Using equation 3.25, equation 3.20 takes the following form:

$$u\frac{\partial u}{\partial x} + v\frac{\partial v}{\partial y} = g\beta\,(T - T_\infty) + \nu\frac{\partial^2 u}{\partial y^2} \tag{3.26}$$

Furthermore, assuming the fluid as an ideal gas, with equation of state $p = \rho RT$, the volumetric temperature expansion coefficient can be expressed as:

$$\beta = \frac{(\rho_\infty/\rho) - 1}{T - T_\infty} = \frac{(T/T_\infty) - 1}{T - T_\infty} = \frac{1}{T_\infty} \tag{3.27}$$

Utilizing the similarity theory, the following characteristic sizes are defined:

$$X = \frac{x}{L_0}, \quad Y = \frac{y}{L_0}, \quad U = \frac{u}{U_0}, \quad V = \frac{v}{V_0}, \quad \theta = \frac{T - T_\infty}{T_s - T_{infty}}, \tag{3.28}$$

where T_s is the temperature on the wall surface. Substituting these variables to equation 3.26 lead to:

$$U\frac{\partial U}{\partial X} + V\frac{\partial V}{\partial Y} = \frac{g\beta\,(T_s - T_\infty)\,L_0}{U_0^2}\theta + \frac{1}{Re}\frac{\partial^2 V_0}{\partial Y^2} \tag{3.29}$$

In this formula the term Gr can be transformed into:

$$\frac{g\beta L^3\,(T_s - T_\infty)\,/\nu^2}{(L_0 U_0/\nu)^2} = \frac{Gr}{Re^2} \tag{3.30}$$

The symbol Gr is called the Grashof number. The Grashof number expresses the buoyant to the viscous forces and is defined as:

$$Gr = \frac{g\beta L^3 \left(T_s - T_\infty\right)}{2} \tag{3.31}$$

The forced and natural convection, commonly, coexist. A useful method to determine the prevailing type of convection is by comparing the Grashof to the Reynolds numbers. If the two numbers are similar, then both forced and natural convection are of equal importance and we have to treat them separately. The Nusselt number depends on the Reynolds, Grashof and Prandtl number. In other cases, when $Gr/Re^2 << 1$, the heat transfer is mainly happening due to forced convection. In contrast, when $Gr/Re^2 >> 1$ natural convection is stronger, and the Nusselt number depends only on the Grashof and Prandtl numbers. In the cases of gases flow, $Pr \approx 1$ and therefore, the Nusselt number is a function of the Grashof number only. Several empirical approaches relate the geometry and the inclination of solid surfaces to the heat transfer coefficient, and can be found in [53, 55]

3.2.3 Thermal Radiation

Thermal radiation is the third mechanism of heat transfer between two bodies. A third body, which acts as a transfer medium is not necessary, and actually it decreases the energy transferred. To emit thermal radiation, a body must have a temperature over 0 K. The amount of the radiative heat of a perfect emitter is a function of its temperature:

$$\dot{q_s} = \sigma T^4, \tag{3.32}$$

where $\sigma = (5.670400 \pm 0.00004)10^{-8} W/m^2K^4$ is the Stefan-Boltzmann constant [55]. The *black body* is considered as a perfect emitter. All other bodies have a reduced capability of emitting thermal radiation, which depends on the material, the temperature and the surface. The decline in radiation emission capability is expressed with the emissivity coefficient ϵ. This coefficient takes values from 0 to 1. Equation 3.33 becomes:

$$\dot{q_s} = \epsilon(T)\sigma T^4, \tag{3.33}$$

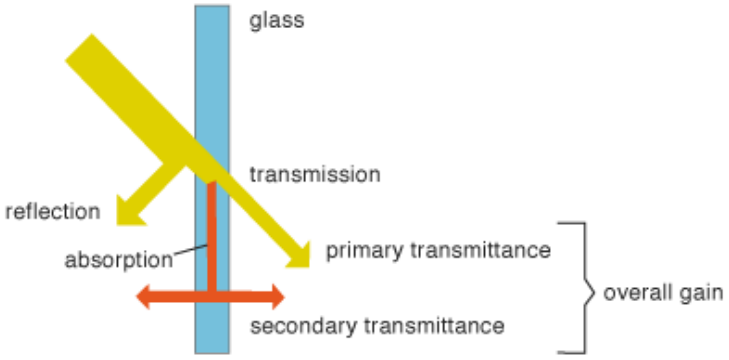

Figure 3.4 Thermal radiation in a case of window [56]

The amount of heat that will be emitted from a surface is calculated as:

$$\dot{Q_{em}} = A\epsilon(T)\sigma T^4 \tag{3.34}$$

On the other hand, a body also receives heat ($\dot{Q_{rc}}$) from thermal radiation. One part of this energy will be absorbed, another will be reflected and a third will be transmitted. It is convenient to use coefficients, which sum to unity, to measure the individual parts of energy. Reflectivity (r), absorptivity (a), and transmissivity (τ) are used and depend on the material and the surface of the object, as well as, from the kind of radiation:

$$r + a + \tau = 1 \tag{3.35}$$

A body will absorb radiation, according to its surface, its absorptivity coefficient and the temperature of the radiative object (T_s) :

$$\dot{Q_{ab}} = Aa\sigma T_s^4 \tag{3.36}$$

A transparent object, in example a window, will also reflect and an amount of energy and let the remaining pass through, figure 3.4 [56]. Usually, the solar energy transmittance of glass(Q_{tr}) is of great importance. Therefore, a coefficient is mentioned along with the other properties; the g-value. The energy passing through is:

$$\dot{Q_{tr}} = g_v \dot{Q_{rc}} \tag{3.37}$$

In contrast, an opaque object will not let any radiation through it. Thus, transmissivity

will be zero. Then, the sum of reflectivity and absorptivity will be unity $a = 1 - r$.

It is clear, that a body will emit and receive thermal radiation at the same time. The net flow heat from this body to the surroundings will be:

$$\dot{Q} = \dot{Q_{em}} - \dot{Q_{ab}} = A\sigma \left(\epsilon T^4 - aT_S^4\right) \tag{3.38}$$

It is common to consider an approximation $a = \epsilon$; the case of the grey body. Thus, the above equation becomes:

$$\dot{Q} = A\sigma\epsilon \left(T^4 - T_S^4\right) \tag{3.39}$$

Another matter to address to, is the cases where both convection and radiation contribute to the heat transfer. The heat flux is:

$$\dot{q} = \dot{q_{conv}} + \dot{q_{rad}} = h(T - T_{air}) + \epsilon \left(T^4 - T_S^4\right), \tag{3.40}$$

where T_{air} denotes the air temperature, which is close to the radiator temperature, thus:

$$\dot{q} = h + h_{rad}(T - T_S), \tag{3.41}$$

where h_{rad} is the radiative heat transfer coefficient:

$$h_{rad} = \epsilon\sigma \frac{T^4 - T_S^4}{T - T_S} = \epsilon\sigma \left(T^2 + T_S^2\right)(T + T_S) \tag{3.42}$$

The quantity h_{rad} can serve as a means to compare the heat transferred from thermal radiation and convection. Note that ϵ is always lower than 1, setting an upper limit in the contribution of radiation in heating [55].

3.2.4 Overall heat transfer

In many cases, the heat transfer between two fluids which are separated by a solid body has to be calculated. As illustrated in figure 3.5, first the warm fluid heats one side of the body, due to convection (red line). Then, the heat is conducted from one side of the body to the other (dotted line). Finally, the heat is transferred to the cold fluid(blue line). The heat flow is calculated as:

$$\dot{Q} = UA(T_{air1} - T_{air2}), \tag{3.43}$$

where U represents the overall heat transfer coefficient, with units (W/m^2K), A is the surface of the body, while *air1* and *air2* denote the warm and the cold air respectively.

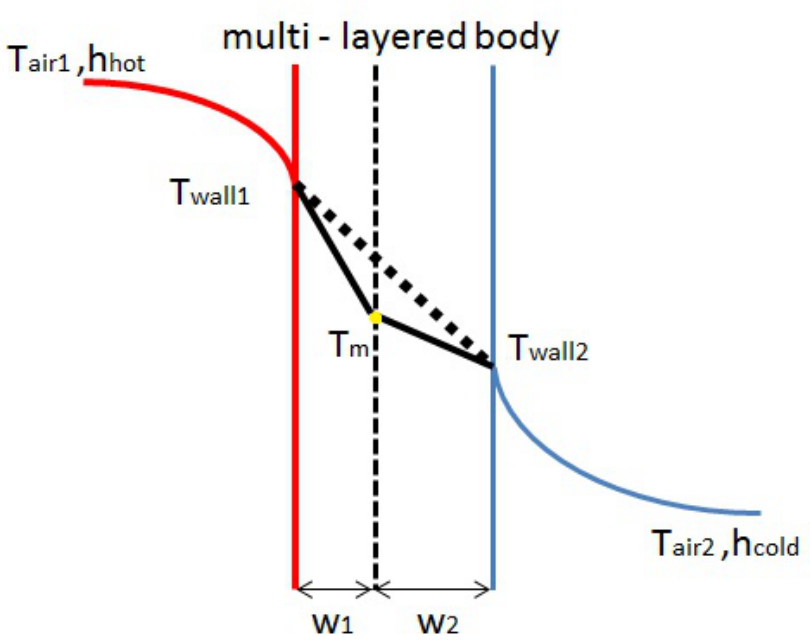

Figure 3.5 Heat transfer through a multi-layered body

In equation 3.43, the geometric and the temperature values can in general be known. The overall heat transfer coefficient (U) is yet to be defined. For this purpose, the heat transfer procedure is divided into three parts. The first part is the convection between the hot air and the left side of the body:

$$\begin{aligned} \dot{Q} &= h_{hot}(T_{air1} - T_{wall1}) \Rightarrow \\ T_{wall1} &= T_{air1} - \frac{\dot{Q}}{h_{hot}} \end{aligned} \tag{3.44}$$

The same procedure is followed for the convection mechanism on the right side of the body:

$$\begin{aligned} \dot{Q} &= h_{cold}(T_{wall2} - T_{air2}) \Rightarrow \\ T_{wall2} &= \frac{\dot{Q}}{h_{cold}} + T_{air2} \end{aligned} \tag{3.45}$$

Finally, the conduction is calaculated:

$$\dot{Q} = \frac{k}{w}(T_{wall1} - T_{wall2}) \tag{3.46}$$

Note that in all equations, the surface of the body is assumed unity without losing generality.

Also, w is the total thickness of the body and the thermal conductivity (k) is assumed constant to the temperature. In equation 3.46, the temperature on the wall is substituted by the values according to the equations 3.44 and 3.45:

$$\begin{aligned}
\dot{Q} &= \frac{k}{w}\left(T_{air1} - \frac{\dot{Q}}{h_{hot}} - \frac{\dot{Q}}{h_{cold}} - T_{air2}\right) \Rightarrow \\
\dot{Q} &= \frac{k}{w}\left(T_{air1} - T_{air2}\right) - \frac{k}{w}\left(\frac{\dot{Q}}{h_{hot}} + \frac{\dot{Q}}{h_{cold}}\right) \Rightarrow \\
\dot{Q}\left[1 + \frac{k}{w}\left(\frac{1}{h_{hot}} + \frac{1}{h_{cold}}\right)\right] &= \frac{k}{w}\left(T_{air1} - T_{air2}\right) \Rightarrow \\
\dot{Q} &= \frac{k/w}{1 + \frac{k/w}{h_{hot}} + \frac{k/w}{h_{cold}}}\left(T_{air1} - T_{air2}\right) \Rightarrow \\
\dot{Q} &= \frac{1}{k/w + \frac{1}{h_{hot}} + \frac{1}{h_{cold}}}\left(T_{air1} - T_{air2}\right) \qquad (3.47)
\end{aligned}$$

Comparing equation 3.47 to 3.43 we can see that the overall that transfer coefficient is:

$$U = \frac{1}{k/w + \frac{1}{h_{hot}} + \frac{1}{h_{cold}}}, \qquad (3.48)$$

or in a form more convenient for calculations:

$$\frac{1}{U} = \frac{1}{h_{hot}} + \frac{w}{k} + \frac{1}{h_{cold}} \qquad (3.49)$$

A similar scheme is used in order to calculate the total thermal conductivity in multi - layer bodies. Initially, the heat flows (black solid line) through the left body, heating the interface (dashed line) to a temperature of T_m. Then, the heat is transferred along the second body to the right wall. The conduction among bodies placed alongside can be calculated as in equation 3.46. By considering each part individually, and the surface as unity, we get the following:

$$\begin{aligned}
\dot{Q} &= \frac{k_1}{w_1}(T_{wall1} - T_m) \Rightarrow \\
T_{wall1} &= \frac{w_1}{k_1}\dot{Q} + T_m, \qquad (3.50)
\end{aligned}$$

and similarly

$$\dot{Q} = \frac{k_2}{w_2}(T_m - T_{wall2}) \Rightarrow$$
$$T_{wall2} = T_m - \frac{w_2}{k_2}\dot{Q} \tag{3.51}$$

Replacing these values to equation 3.46 yields:

$$\dot{Q} = \frac{k}{w}\left(\frac{w1}{k1}\dot{Q} + \frac{w2}{k2}\dot{Q}\right) \Rightarrow$$
$$\frac{w}{k} = \frac{w1}{k1} + \frac{w2}{k2} \tag{3.52}$$

Hence, equation 3.46 takes the following form:

$$\dot{Q} = \left(\frac{w1}{k1} + \frac{w2}{k2}\right) A(T_{wall1} - T_{wall2}), \tag{3.53}$$

or considering N number of bodies

$$\dot{Q} = \sum_{i=1}^{N} \frac{w_i}{k_i} A_i(T_{wall1} - T_{wall2}), \tag{3.54}$$

A final estimation of the overall heat transfer coefficient, in general cases, can be calculated from:

$$\frac{1}{UA} = \frac{1}{h_{hot}A_1} + \sum_{i=1}^{N} \frac{w_i}{k_i A_i} + \frac{1}{h_{cold}A_N} \tag{3.55}$$

Conduction in multi - layered bodies is a significant aspect of heat transfer. In order to combine beneficial properties of materials in building applications, a common practice is to employ structure elements consisting of two or more materials. Such examples can be the insulation in walls or a PCM system, especially in the case of macroencapsulation. We employ this method in the next section, to derive the thermal conductivity of the PCM system we study.

3.3 Fluid Dynamics

Any given physical system is limited by three constrains: i) the mass cannot be created or destroyed, but can be rearranged in space and time, ii) the act of a steady force on a body will cause it to accelerate, and iii) the energy is conserved in an isolated system. It is common, to refer to these constrains as the mass conservation, second Newton's law or momentum

conservation and energy conservation principles.

When studying a continuous flow field, two approaches can be considered: the finite control volume and the infinitesimal fluid element, also called the Euler and Lagrange method respectively. Using the first, the values of a specific variable in one individual point, in the physical space during time evolution, can be obtained. The temperature can be considered as characteristic example. On the other hand, when information on a particle property is needed, such as the size of a droplet along its orbit, the Lagrange method is more suitable [57]. Both methods can lead to the same partial differential equations, but are employed considering the provided convenience to describe the investigated characteristics of the system.

In the cases studied in the next chapter, the fluid is air is treated as an ideal gas. This means that it obeys the equation of state

$$pV = nRT \tag{3.56}$$

Here p is the pressure, V is the system volume, n is the number of moles, R is the gas constant equal to 8.314 $J/molK$, and T the temperature. Furthermore, under the consideration of a Newtonian fluid the shear stress tensor is connected to the shear strain as:

$$\tau_{ii} = \lambda \nabla \cdot \vec{V} + 2\mu \frac{\partial u_i}{dx_i}, \tag{3.57}$$

$$\tau_{ij} = \mu \left(\frac{\partial u_i}{dx_j} + \frac{\partial u_j}{dx_i} \right), i \neq j, \tag{3.58}$$

where λ is the bulk viscosity coefficient and μ is the dynamic viscosity. These two quantities are connected through the Stokes hypothesis as:

$$\lambda = -\frac{2}{3}\mu \tag{3.59}$$

The set of the Navier - Stokes equations are:

- The continuity equation:

$$\frac{\partial \rho}{\partial t} + \nabla \cdot \left(\rho \vec{V} \right) = 0, \tag{3.60}$$

- The momentum equation:

x- direction

$$\frac{\partial(\rho u)}{\partial t}+\frac{\partial\left(\rho u^{2}\right)}{\partial x}+\frac{\partial\left(\rho u v\right)}{\partial y}+\frac{\partial\left(\rho u w\right)}{\partial z}= \\ -\frac{\partial p}{\partial x}+\frac{\partial}{\partial x}\left(\lambda\nabla\cdot\vec{V}+2\mu\frac{\partial u}{\partial x}\right) \\ +\frac{\partial}{\partial y}\left[\mu\left(\frac{\partial v}{\partial x}+\frac{\partial u}{\partial y}\right)\right]+\frac{\partial}{\partial z}\left[\mu\left(\frac{\partial u}{\partial z}+\frac{\partial w}{\partial x}\right)\right]+\rho F_{x} \tag{3.61}$$

y- direction

$$\frac{\partial(\rho v)}{\partial t}+\frac{\partial\left(\rho u v\right)}{\partial x}+\frac{\partial\left(\rho v^{2}\right)}{\partial y}+\frac{\partial\left(\rho v w\right)}{\partial z}= \\ -\frac{\partial p}{\partial y}+\frac{\partial}{\partial y}\left(\lambda\nabla\cdot\vec{V}+2\mu\frac{\partial v}{\partial y}\right) \\ +\frac{\partial}{\partial x}\left[\mu\left(\frac{\partial v}{\partial x}+\frac{\partial u}{\partial y}\right)\right]+\frac{\partial}{\partial z}\left[\mu\left(\frac{\partial w}{\partial y}+\frac{\partial v}{\partial z}\right)\right]+\rho F_{y} \tag{3.62}$$

z- direction

$$\frac{\partial(\rho w)}{\partial t}+\frac{\partial\left(\rho u w\right)}{\partial x}+\frac{\partial\left(\rho v w\right)}{\partial y}+\frac{\partial\left(\rho w^{2}\right)}{\partial z}= \\ -\frac{\partial p}{\partial z}+\frac{\partial}{\partial z}\left(\lambda\nabla\cdot\vec{V}+2\mu\frac{\partial w}{\partial z}\right) \\ +\frac{\partial}{\partial x}\left[\mu\left(\frac{\partial u}{\partial z}+\frac{\partial w}{\partial x}\right)\right]+\frac{\partial}{\partial y}\left[\mu\left(\frac{\partial w}{\partial y}+\frac{\partial v}{\partial z}\right)\right]+\rho F_{z} \tag{3.63}$$

- The energy equation:

$$\frac{\partial(\rho e)}{\partial t}+\nabla\left(\rho e\vec{V}\right)=\rho\dot{q}_{v}+\frac{\partial}{\partial x}\left(k\frac{\partial T}{\partial x}\right)+\frac{\partial}{\partial y}\left(k\frac{\partial T}{\partial y}\right)+\frac{\partial}{\partial z}\left(k\frac{\partial T}{\partial z}\right) \\ -p\left(\frac{\partial u}{\partial x}+\frac{\partial v}{\partial y}+\frac{\partial w}{\partial z}\right) \\ +\lambda\left(\frac{\partial u}{\partial x}+\frac{\partial v}{\partial y}+\frac{\partial w}{\partial z}\right)^{2} \\ +\mu\left[2\left(\frac{\partial u}{\partial x}\right)^{2}+2\left(\frac{\partial v}{\partial y}\right)^{2}+2\left(\frac{\partial w}{\partial z}\right)^{2}\right. \\ \left.+\left(\frac{\partial u}{\partial y}+\frac{\partial v}{\partial x}\right)^{2}+\left(\frac{\partial u}{\partial z}+\frac{\partial w}{\partial x}\right)^{2}+\left(\frac{\partial v}{\partial z}+\frac{\partial w}{\partial y}\right)^{2}\right. \tag{3.64}$$

where $\vec{V}$ is the fluid velocity, u,v,w the components of the velocity, e the internal energy and $\dot{q}_{v}$ is the additional volumetric heat rate per unit mass [9].

To conclude, it is common in fluid dynamics to calculate the Reynolds number, which is

defined as:

$$Re = \frac{\rho u_0 L_0}{\mu} \tag{3.65}$$

The magnitude of the Reynolds numbers indicates, whether a flow is laminar or turbulent. In a boundary layer flow over a flat plate experiments confirm that turbulence is observed for a Reynolds number of 5×10^5. In cases where natural convection is dominant the characteristic velocities are quite small leading to laminar flows. Therefore, no treatment for turbulence was employed.

3.4 Numerical modeling of the problem

In the previous sections, the physical problem was presented in terms of mathematical expression, through the heat transfer and the Navier-Stokes equations. In general, the analytical-exact solution of this system of partial differential equations is proved to be a tedious procedure, possible only for simple cases, such as the Couette flow.

To handle complicated cases, where the non-linearity of the equations prevents the derivation of the exact solution, numerical methods have been employed over the past 50 years. The goal of these methods, is to provide a solution as close as possible to the real one. At first only small systems could be handled, but with the growing computational power large scale systems can now be simulated.

In this work, the finite volume method is adopted, which is claimed as one of the methods to impose naturally the conservation laws in their integral form [9]. Various topics are discussed: the process of discretizing the equations, the boundary conditions, as well as, time marching problems and stability. Comments on grid generation conclude this part.

3.4.1 Formulation of equations using the Finite Volume Method

The first step, is to divide the geometry of the physical domain into smaller sections, a process called the grid generation. In the beginning, the length in each dimension is divided into a number of line segments. Then, the faces of the geometry are divided into individual areas, and finally the volume is sorted into a number of smaller volumes. The intersection of line segments define a numerical node. Each node is contained in a control volume, also called computational cell. We illustrate this procedure in figure 3.6. The example shows a two dimensional rectangular domain, for convenience reasons without losing generality. We indicate a computational cell with dashed lines, n the bottom figure. The capital letters denote the nodes, while the lowercase is used to represent the boundary of the volume cell. The

differential equations are integrated over these cells and then discretized, leading to a number of algebraic equations, which are solved on the nodes.

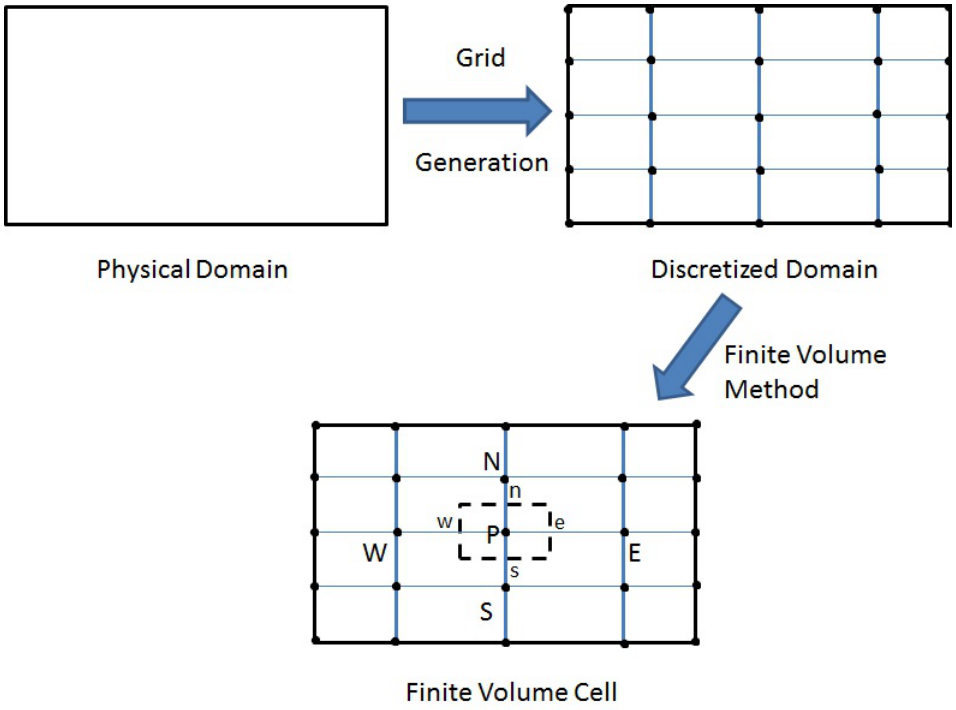

Figure 3.6 Grid generation on a 2D rectangular physical domain

To set an example, a cell showed above is enlarged and the characteristic lengths are defined, figure 3.7. Also, a simple heat transfer equation with conduction is discretized, which can be expressed by the Laplace equation:

$$\frac{\partial}{\partial x}\left(k\frac{\partial T}{\partial x}\right)+\frac{\partial}{\partial y}\left(k\frac{\partial T}{\partial y}\right)=0 \tag{3.66}$$

First, the above equation is integrated on the specific control volume:

$$\int\int_{enws}\frac{\partial}{\partial x}\left(k\frac{\partial T}{\partial x}\right)dxdy+\int\int_{enws}\frac{\partial}{\partial y}\left(k\frac{\partial T}{\partial y}\right)=0 \tag{3.67}$$

The first term can be written as:

$$\int\int_{enws}\frac{\partial}{\partial x}\left(k\frac{\partial T}{\partial x}\right)dxdy=\int_{e}\left(k\frac{\partial T}{\partial x}\right)dy-\int_{w}\left(k\frac{\partial T}{\partial x}\right)dy, \tag{3.68}$$

and by applying the mean value theorem, while assuming a constant k in each direction:

$$\overline{\left(k\frac{\partial T}{\partial x}\right)}_{e}\delta y_e-\overline{\left(k\frac{\partial T}{\partial x}\right)}_{w}\delta y_w=k_e\frac{T_E-T_P}{\Delta x_{PE}}\delta y_e-k_w\frac{T_P-T_W}{\Delta x_{PW}}\delta y_w \tag{3.69}$$

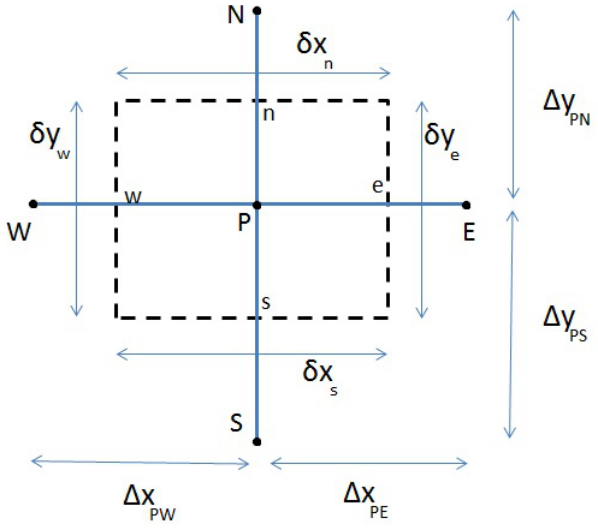

Figure 3.7 Characteristic finite volume computational cell

By applying the same on the right term of equation 3.67 a similar expression is derived for the y-axis:

$$\int\int_{enws} \frac{\partial}{\partial y}\left(k\frac{\partial T}{\partial y}\right) dxdy = k_n \frac{T_N - T_P}{\Delta y_{PN}} \delta x_n - k_s \frac{T_P - T_S}{\Delta y_{PS}} \delta x_s \tag{3.70}$$

Combining the right terms of the last two equations leads to:

$$k_e \frac{T_E - T_P}{\Delta x_{PE}} \delta y_e - k_w \frac{T_P - T_W}{\Delta x_{PW}} \delta y_w + k_n \frac{T_N - T_P}{\Delta y_{PN}} \delta x_n - k_s \frac{T_P - T_S}{\Delta y_{PS}} \delta x_s = 0 \tag{3.71}$$

It is more convenient to write the last equation in the form:

$$C_E T_E + C_W T_W + C_S T_S + C_N T_N = C_P T_P, \tag{3.72}$$

by defining the coefficients as:

$$C_E = \frac{k_e \delta y_e}{\Delta x_P E}, \quad C_W = -\frac{k_w \delta y_w}{\Delta x_P W}, \quad C_S = -\frac{k_s \delta x_s}{\Delta y_P S}, \quad C_N = \frac{k_n \delta x_n}{\Delta y_P N} \tag{3.73}$$

The coefficient C_P is the sum of the rest coefficient, namely: $C_P = C_E + C_W + C_S + C_N$. This procedure is applied, also, in three dimensional cases. Note that, equation 3.72 is valid for every node *inside* the descritized domain. Nodes on the borders have to be treated separately by the boundary conditions.

3.4.2 Boundary conditions

Notably, the Navier-Stokes, as well as, the heat transfer equations are valid in every physical domain, assuming the continuity is valid. However, among physical domains different aspects

can be observed. The special ingredient of each individual case is the boundary conditions, which apply to the *outermost* nodes of the domain. As such, they are treated separately from the rest of nodes.

Three types exist: the Diriclhlet, the Neumann and the mixed type. The first are imposed by assigning the known value of the boundary directly to the boundary nodes. For the remaining two, separate equations have to be solved along with equation 3.72. To demonstrate the form of the additional equations, a mixed boundary condition is assumed:

$$-k\frac{\partial T}{\partial x}_{w} = h\left(T_{\infty} - T_{B}\right), \tag{3.74}$$

where T_{∞} is the environment temperature and T_B the temperature along the left wall in figure 3.8.

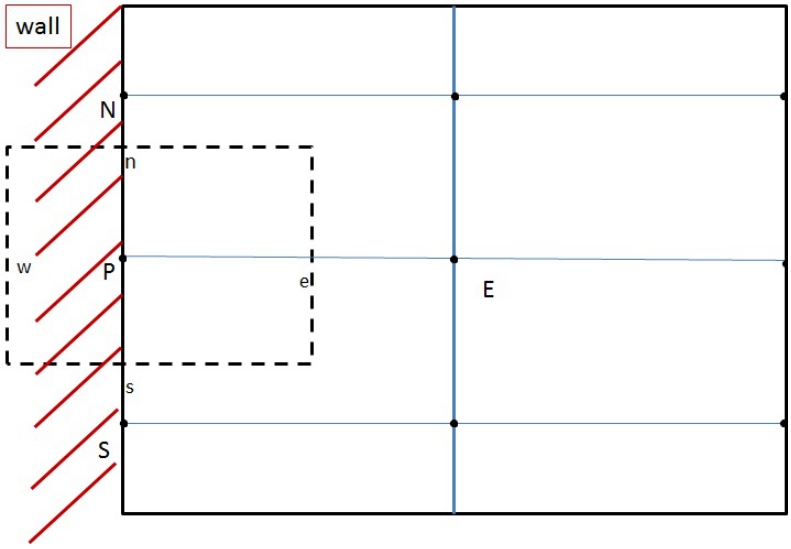

Figure 3.8 Domain with wall on the left boundary

The procedure used to obtain equation 3.72 will be followed:

- in the x-axis:

$$\begin{aligned}\frac{\partial}{\partial x}\left(k\frac{\partial T}{\partial x}\right) &= \int_{e} k\frac{\partial T}{\partial x}dy - \int_{w} k\frac{\partial T}{\partial x}dy \\ &= k_e\frac{T_E - T_P}{\Delta x_{PE}}\delta y_e - h\left(T_{\infty} - T_B\right)\end{aligned} \tag{3.75}$$

- in the y-axis the result will be the same as in equation 3.70

The final result will be similar to equation 3.72:

$$C_E T_E + C_S T_S + C_N T_N = C_P T_P + b, \tag{3.76}$$

where

$$C_E = \frac{k_e \delta y_e}{\Delta x_P E}, \quad C_S = -\frac{k_s \delta x_s}{\Delta y_P S}, \quad C_N = \frac{k_n \delta x_n}{\Delta y_P N} \quad , C_P = C_E + C_S + C_N - h, \; b = hT_\infty \tag{3.77}$$

To sum up, in order to obtain the solution for the whole domain, equation 3.72 (for the inner nodes), and equation 3.76 (for the boundary nodes) have to solved in a combined way.

3.4.3 Transient problems

In many cases, it is important to capture the behaviour of a phenomenon in the evolution of time. Time dependent problems can be modeled in the same fashion described for the grid generation. The time margin (t_d) is divided in number (N_t) of time steps, leading to a time interval (Δt) of $\Delta t = t_d/N_t$. In this work, the upper index n refers to the current value of the variable, and $n+1$ to the value to be calculated at the next moment.

To make the description easier, in the following example,a one dimensional problem is presented:

$$\rho c_p \frac{\partial T}{\partial t} = \frac{\partial}{\partial x}\left(k \frac{\partial T}{\partial x}\right) \tag{3.78}$$

To make the integration procedure easier, the density, heat coefficient, and conductivity are assumed to be constant through time and with the temperature fluctuation. After the integration in time and space the following expression is derived:

$$\rho c_p \int_w^e \int_t^{t+\Delta t} \frac{\partial T}{\partial t} dt dx = \int_t^{t+\Delta t} \int_w^e \frac{\partial}{\partial x}\left(k \frac{\partial T}{\partial x}\right) \Rightarrow \tag{3.79}$$

$$\rho c_p \left(T_P^{n+1} - T_P^n\right) = \int_t^{\Delta t} \left[\frac{k_e}{\delta x_e}\left(T_E - T_P\right) - \frac{k_w}{\delta x_w}\left(T_P - T_W\right)\right] dt \tag{3.80}$$

At this point, a relation on the time dependent variable has to be enforced between the nodes E,P and W. A common expression is [58]:

$$\int_t^{t+\Delta t} T_P dt = \left[\omega T_P^{n+1} + (1-\omega) T_P^n\right] \Delta t, \tag{3.81}$$

where ω is a weight coefficient, which values will be examined later. Hence, equation 3.79 becomes:

$$\begin{aligned} \rho c_p \int_w^e \int_t^{t+\Delta t} \frac{\partial T}{\partial t} dt dx = \omega & \left[\frac{k_e}{\delta x_e}\left(T_E^{n+1} - T_P^{n+1}\right) - \frac{k_w}{\delta x_w}\left(T_P^{n+1} - T_W^{n+1}\right)\right] \\ & + (1-\omega)\left[\frac{k_e}{\delta x_e}\left(T_E^n - T_P^n\right) - \frac{k_w}{\delta x_w}\left(T_P^n - T_W^n\right)\right] \end{aligned} \tag{3.82}$$

The last equation is expressed in a more compact from:

$$a_p^* = a_E \left[\omega T_E^{n+1} + (1-\omega)T_E^n\right] + a_W \left[\omega T_W^{n+1} + (1-\omega)T_W^n\right] + \left[a_P - (1-\omega)a_E - (1-\omega)a_W\right] T_P^N, \tag{3.83}$$

where

$$a_E = \frac{k_e}{\delta x_e}, \quad a_W = \frac{k_w}{\delta x_w}, \quad a_P = \frac{\rho c_p \Delta x}{\Delta t} \quad \text{, and} \quad a_P^* = a_P + \omega a_E + \omega a_W \tag{3.84}$$

Examining the weight coefficient ω, a zero value leads to an explicit numerical scheme, whereas for unity the scheme is implicit. Intermediate values lead to a complex scheme of Crank-Nicholson type. Implicit schemes are in general faster to solve and more stable [57]. However, with the growing development of parallel processing explicit schemes are becoming popular. Nevertheless, to meet stability needs, the Courant-Fridriech-Levy (CFL) condition has to be met. In example, in the special occasion of constant thermal conductivity ($k = k_e = k_W$) and discretization ($\Delta x = \delta x_e = \delta x_w$) in both directions, this condition states that the following criterion should be applied:

$$\alpha \frac{\Delta t}{\Delta x} \leq \frac{1}{2} \tag{3.85}$$

, where $\alpha = \frac{k}{\rho c_p}$ [53].

For the momentum equation the stability criterion is different, and the theoretical analysis is out of the scope of this thesis. A first selection of time step can be made following the expression:

$$u \frac{\Delta t}{\Delta x} \leq \frac{1}{2}, \tag{3.86}$$

where u is a characteristic velocity. A useful introduction in [9], where the Runge-Kutta and the multi-stage time stepping are discussed, is recomended for the interested reader.

3.4.4 Aspects of grid generation

To create a grid that "fits" in a physical domain, two approaches can be considered: the structured and the unstructured meshing. In the first, the nodes are numbered successively, while in the second additional lists are used to store the position of the individual nodes and edges. The second method seems more cumbersome to achieve and manage, nevertheless it provides a great advantage over the first: it can be used to mesh any given geometry, due to the fact that several cells can be used to fill a given domain, showed in figure 3.9 [9]. Most

commercial software package adopt the unstructured meshing [9].

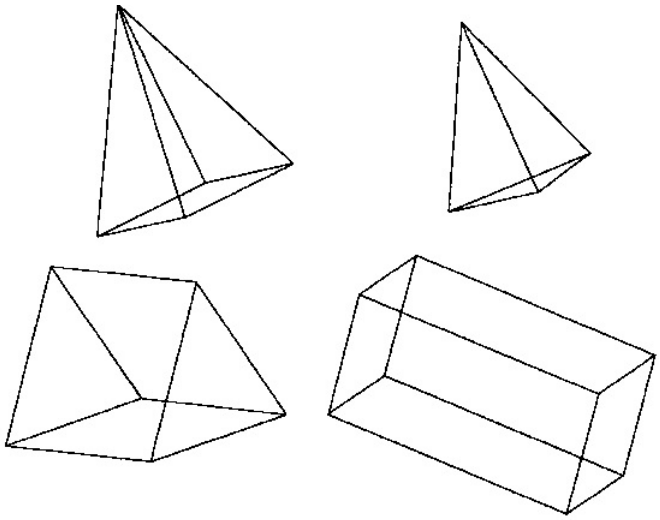

Figure 3.9 Cells used to create an unstructured mesh [9]

In general, it is acceptable to claim that, accuracy of the solution is enhanced, as the mesh becomes more dense. This treatment leads to a large amount of nodes, in which the algebraic equations are solved. However, this path cannot be followed in every situation, as there is an upper limit to the number of calculation processed in a specific time, and the available memory. To put it simply, the computational cost has to be assessed, before simulating the real problem. Here, some useful criteria on how to create an efficient grid are mentioned.

First of all, the nature of the physical problem set some restrictions to the calculations. In example, in case where a boundary layer is present, a large number of nodes are needed close to the boundary, to be able to compute the values of the characteristic properties of the flow in that specific area. However, this less nodes can be considered sufficient, depending on the case, for the rest of the computations in the remaining domain. Hence, different density of nodes in the grid have to be imposed in different regions. Secondly, the orientation of the mesh should follow the direction of the flow, as much as possible, to avoid numerical diffusion, an issue described in [9, 57]. Another aspect is to avoid too sharp or too blunt contact angles between the computational cells. This implementation can cause a low quality mesh, leading to numerical inaccuracies. Finally, it is possible that the phenomenon studied, changes position throughout the time evolution. A typical case is a shock wave, where the large derivatives have to be captured by a dense mesh. In this case, the same high density of nodes can be imposed in a steady mesh, or implement an adaptive mesh that is subjected to the position of the fast altering derivatives, while being more dilute in the rest of the domain. In any case given, it is favourable to compare results obtained with different meshes, in order to use the most efficient.

In this work, the grids generated are two dimensional, and almost in all regions orthogonal elements are implemented. In the first case, the grid is a bit more dense close to the PCM system. In the second, a homogeneous discretization has been imposed, to allow better accuracy throughout the whole domain.

4 Numerical study of a phase change material system

This chapter consists of three parts. In the first, we present and evaluate our numerical method. The experiment presented in [35], and briefly described here, is used as a validation case. We choose this work for a number of reasons:

i. the purpose of this work was to demonstrate benefits upon installation of PCM systems in buildings,
ii. radiation and natural convection are the main mechanisms for heat transfer, and
iii. accurate boundary conditions and results are provided

The equations, discussed in the previous section, are handled with a commercial software (CFX). The software uses the finite volumes method and the solution takes place in a refined two dimensional grid. We consider the properties of the materials constant, with the exception of the heat transfer coefficient, which we model with the effective heat capacity method. In addition, the initial and boundary conditions are imposed with care from the experiment.

A discussion on the results is necessary to validate our model. Convergence has proven a difficult task. However, the trend, expressed in terms of polynomial fitting, is comparing well with the actual values. This led to proceed to a prediction case.

The fundamental purpose of this work is to investigate how the installation of a PCM application affects the thermal behaviour of an already existing outer building wall. This consists the prediction case in this work. A wall is heated from the thermal radiation of the environment. The purpose of the installation of a phase change material system is twofold: providing thermal protection in summer, and minimizing heat loss in winter. Therefore, we investigate the specific system under two different temperature and radiation conditions. We compare two configurations of the system. The modeling procedure is similar to the validation case, although we investigate only steady cases. The results will show the beneficial impact of the PCM on preventing an overwhelming temperature increase. However, transient simulations are needed to confirm further assumptions.

Finally, the last part sums up the simulations findings and provides suggestions for ongoing work.

4.1 Phase change material integrated in a blind

4.1.1 Experimental setup

Initially, we introduce the properties of the used PCM, namely Delta® -Cool 28 produced by Dörken company. The specific melting enthalpy and the melting range, are 188 kJ/kg and 26-30 °C respectively. The thermal conductivity ranges from 0.56 to 1.12 W/mK and the specific heat capacity from 2200 to 2700 J/kgK, depending on the phase (liquid-solid). In addition, it is encapsulated in a hollow polycarbonate container, which thermal conductivity is typically 0.25 [59]. This PCM is integrated to a 20 mm thick sun protection system, which we will refer to it as PCM blind. Furthermore, two main aspects have to be mentioned: i) the PCM blind is covered in a white fabric to reduce its absorption coefficient to 0.22 and ii) the PCM covers 15 out of the 20 mm thickness the application. Below the properties of the PCM blind are sorted in table 4.1 and figure 4.1. The density is considered to be dependent only on the PCM, while the thermal conductivity is calculated using the relation 3.52 for the PCM and the polycarbonate. Finally, figure 4.1 shows the specific heat capacity, which we calculate using the effective heat capacity method, taking into account the melting range and the melting enthalpy.

Table 4.1 Constant properties of PCM blind

density	1500 kg/m^3
thermal conductivity	0.775 W/mK
absorption coefficient	0.220

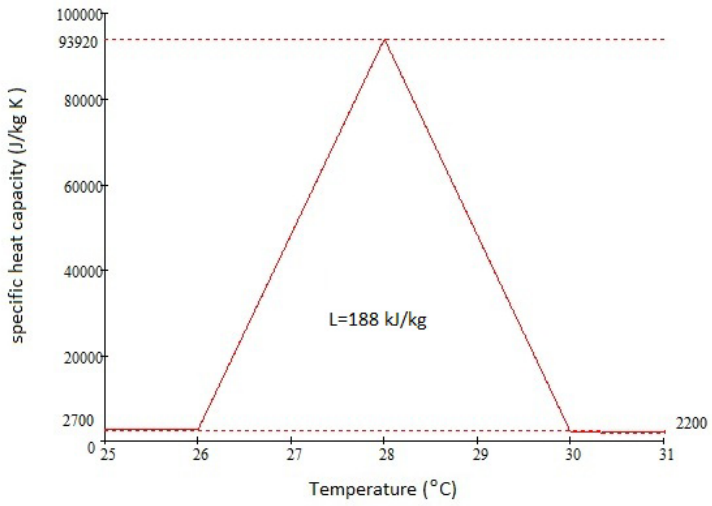

Figure 4.1 Heat transfer coefficient of PCM blind

$$c_p(T) = \begin{cases} 2700 & ,T < 26°C \\ 2700 + 45610\,(T-26) & ,26 \geq T \geq 28°C \\ 2200 - 45900\,(T-30) & ,28 \geq T \geq 30°C \\ 2200 & ,T > 30°C \end{cases} \tag{4.1}$$

The PCM blind was tested in an experimental facility. It was installed in the right chamber, shown in figure 4.2 [35], by placing it to an aluminum holding. The length and height of that chamber are 1.2 and 1.5 m respectively.

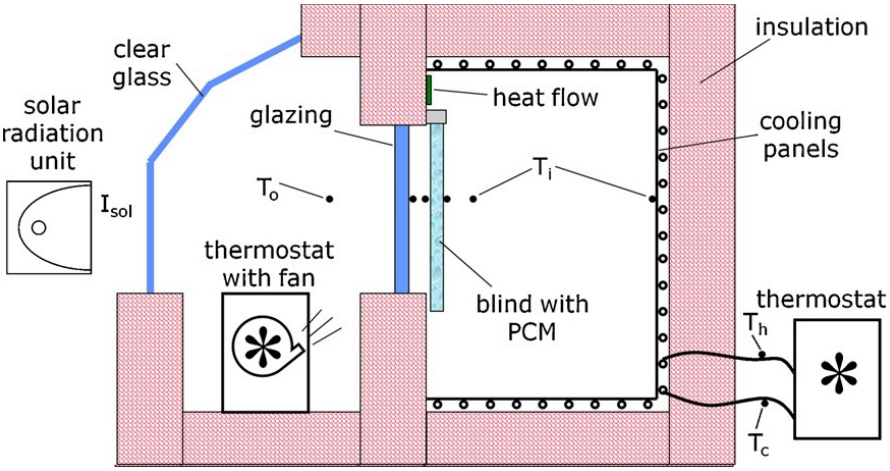

Figure 4.2 Experimental facility to test the PCM blind [35]

The left chamber, in this figure, represents the exterior environment. The temperature in this region is preserved at 25 °C, with the help from the thermostat. Outside this region a solar radiation unit exists. The clear glass let the total amount of irradiation pass without losses. Between the two rooms a doubled glazing with a g-value of 0.6 and U-value 1.3 W/m^2K exists. The blind is placed 15 cm from that glass, leaving a gap of 5 cm from the wall. The top, bottom and side walls of the test room were kept at almost a constant temperature of about 23 to 24 °C, with the help of a thermostat and cooling panels. The rest of the chamber is insulated.

In the beginning of the experiment, the room is at 23 °C. Radiation of intensity 530 W/m^2 hits the glazing. The temperature is measured in various positions: i) at the outside chamber, 5 cm from the glazing, to ensure that the temperature remains at the desirable value, ii) at the glazing, iii) at the outer and inner side (left and right respectively) of the blind, iv) 5 cm from the blind, and v) on the walls. The temperature of the glazing rises to a value of almost 38 °C, within a time period of 2 hours and then rises steadily to 42 °C after 24 hours. The evolution of temperature in the interior at a distance 5 cm from the blind (the left T_i in figure

4.2), is captured. This will be compared to our simulation results. The data from the inner side of the blind will be used to evaluate our results. In addition, the heat flow is measured at the location illustrated in the figure. A heat flow from the test chamber to the outside, of magnitude 1 Watt, was reported.

4.1.2 Computational approach

To simulate the experiment the geometry of the right chamber in figure 4.2 is recreated. The basic geometrical features are illustrated in figure 4.3 .

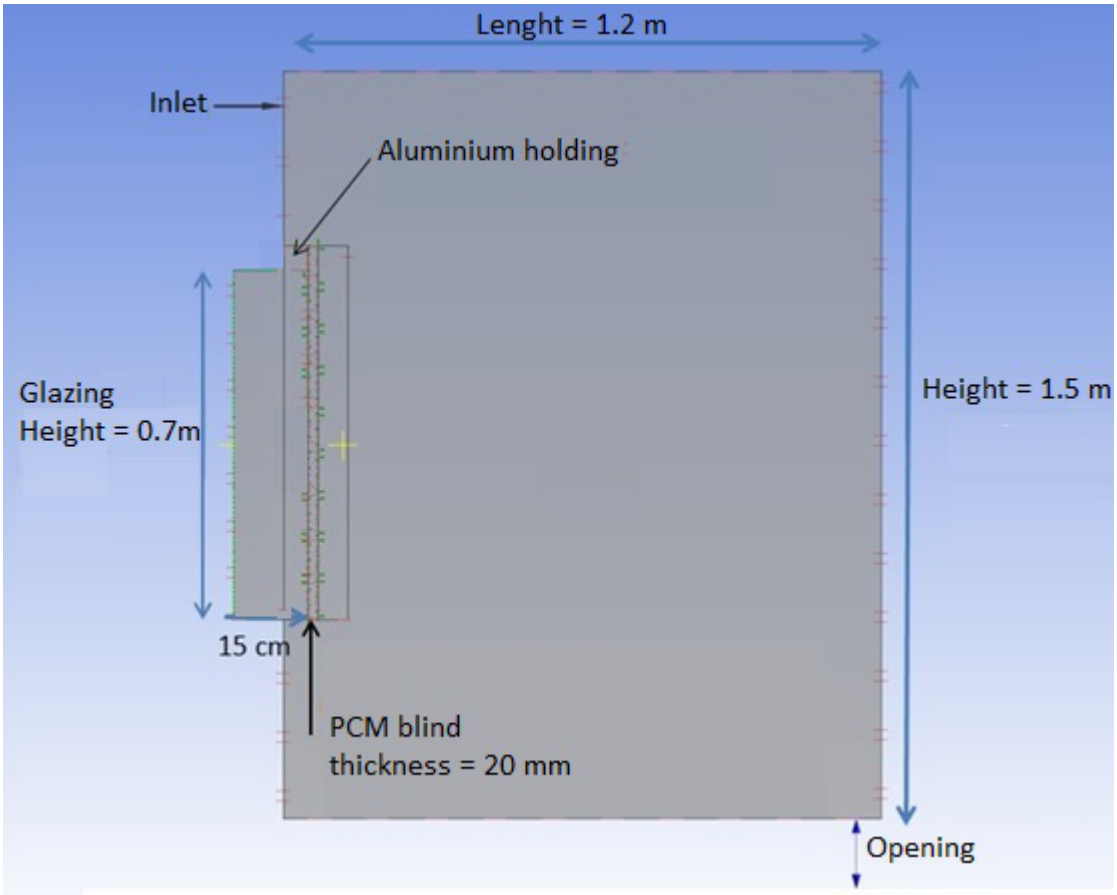

Figure 4.3 Modeling of the experimental chamber

The mesh generation follows the concepts mentioned in the end of the previous chapter, and the grid is illustrated in figure 4.4. Almost all elements, 18820 in total, are rectangular, leading to a fine quality mesh. Note that, on both sides of the blind, shown in yellow and orange, two individual regions are created. These regions contain a denser mesh comparing to the other regions. In example, the distance of the first nodes from the blind on the left side is 8 mm, whereas the elements on the right side have a length of 6 mm. The first reason, for this treatment, is to capture accurately the phenomenon of natural convection near the blind. Additionally, the area in front of the blind allows to mesh smoothly the gap between the blind

and the wall.

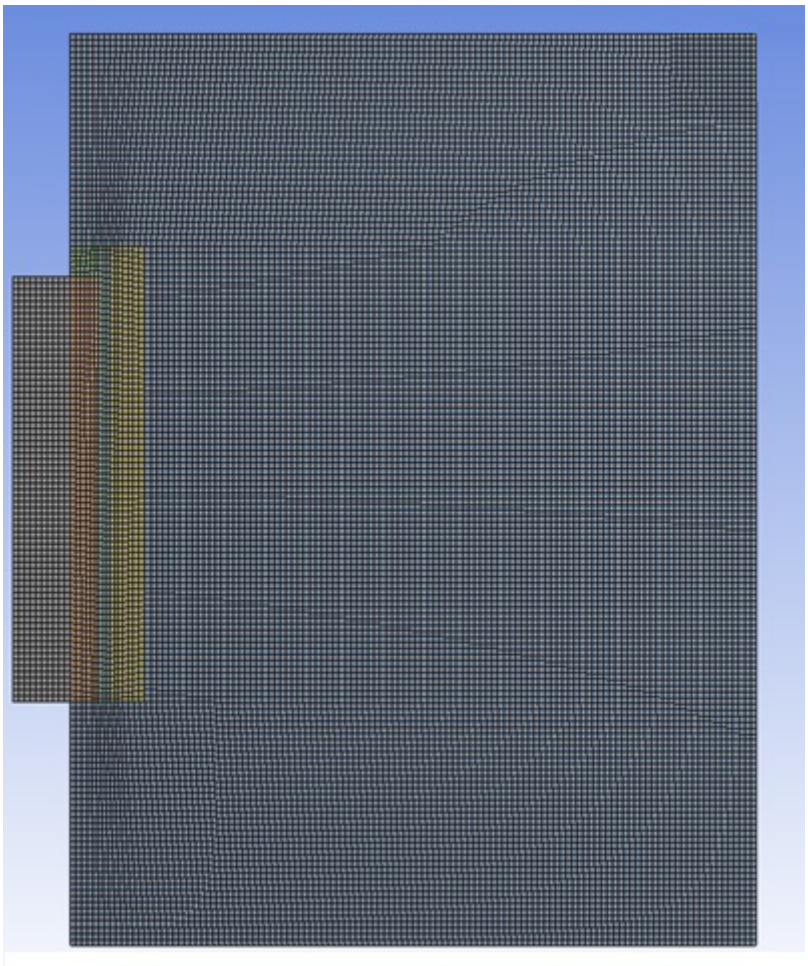

Figure 4.4 Numerical grid of the experimental chamber

The next task, is to define the proper physics to each region of our domain. To handle the PCM blind, a material with the specified properties in table 4.1 and figure 4.1 is defined. The aluminum holding is treated separately, while the rest of the domain is filled with air, treated as an ideal gas. Further on, the buoyancy model is applied, setting the gravity acceleration to 9.81 m/s^2. The radiation is treated with a Monte Carlo model, because it allows to specify both the intensity and the direction. Simply put, the software simulates the interaction between photons and the environment by recording a certain amount of events, which is set to 10000, and subjected to the Poisson statistics. To simplify matters, all radiation quantities are assumed to be uniform, thus the Gray spectrum model is selected. Further information on this model is available in the software's manual [60].

After setting the physical model, the initial and the boundary conditions are imposed. First of all, a special treatment, in order to ensure the stability of the transient simulation, is introduced. A small inlet on the top left of the domain provides a negligible amount of air, with a normal velocity of 0.001 m/s. In addition, an opening at the bottom right with a relative

pressure of 0 Pa allows the air to escape.

In order to implement the initial conditions, a steady case is necessary. The temperature in the whole domain is 23 °C, and a vertical velocity of 0.001 m/s is enforced. Then, the Navier-Stokes equations are solved for a considerable large number of iterations (30000). The temperature and the velocity field of this procedure are viewed in figure 4.5. These are the initial conditions to the transient simulation.

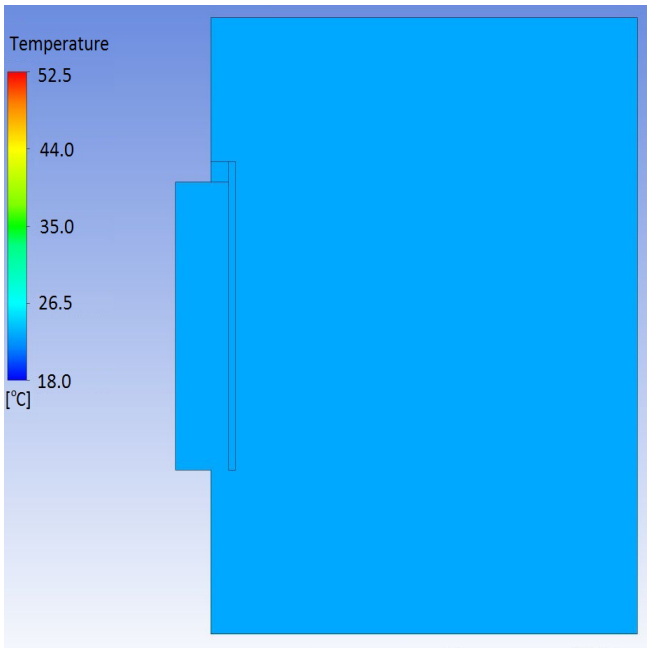

(a) Initial temperature

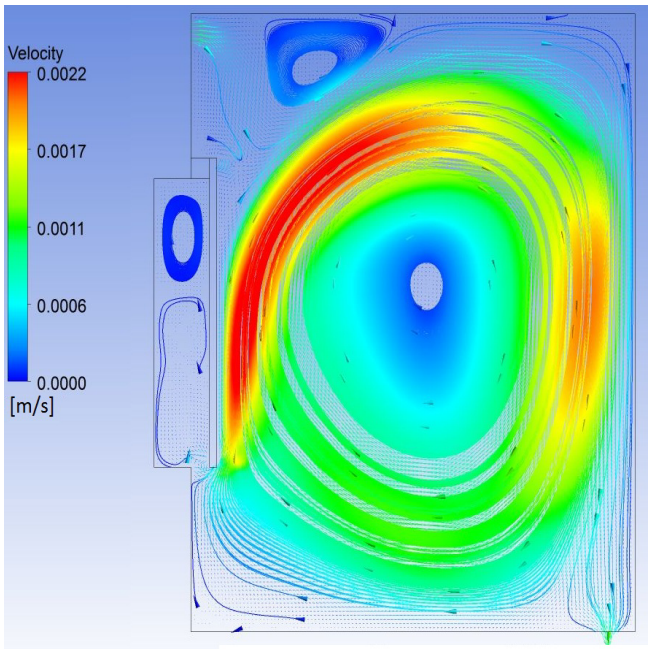

(b) Initial velocity

Figure 4.5 Initial conditions for the transient simulation

The boundary conditions are described next. The glazing is modeled as a wall, from which

a radiative constant heat flux is emitted, with a normal direction to the blind and an intensity of 318 W/m^2, taking into account the g-value. The g-values is a coefficient to measure the ratio of the radiative heat that flows through a transparent object, equation 3.37. The temperature of the glazing is treated, as accurately as possible, from the experimental work. The evolution of temperature on the glazing is showed in figure 4.6. The temperature of the top, bottom and right wall, as well as the inlet and the opening are set to rise linearly from 23 to 24 °C, within a period of 24 hours. The other walls are adiabatic.

In this implementation a basic feature has been omitted: the heat losses from the test to the outside chamber. To elucidate, the U-value has not been treated in this model. This property measures the amount of thermal energy transfer through the window. Thus, no heat is transferred from the chamber through the window. This will lead to a big error, regarding the temperature rise in the region between the glazing and the blind, and to the blind itself. In addition, the walls are considered adiabatic, despite the fact, that heat of 1 Watt flows from the chamber to the outside environment through the walls.

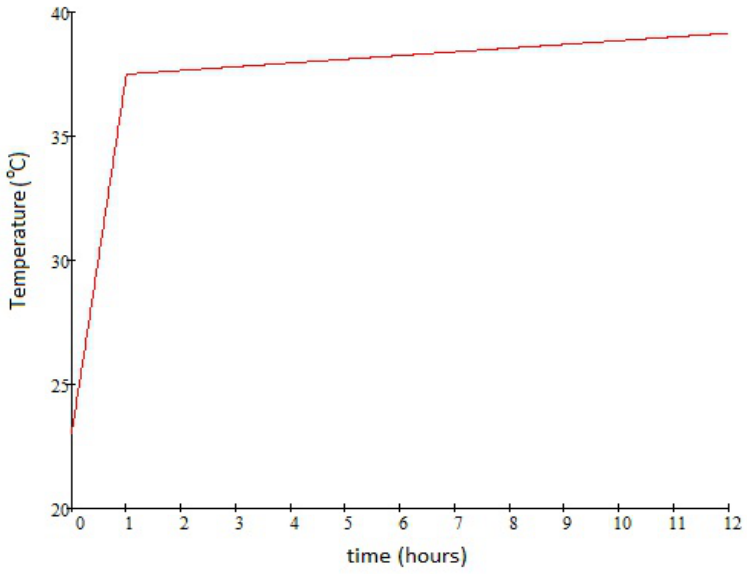

Figure 4.6 Temperature evolution of glazing used as boundary condition

To capture the temperature and the flow field, during the time evolution, a time step of 9 seconds is considered proper based on a first CFL consideration, equation 3.86. The solver is adjusted to perform 20 iteration per time step, to solve the conservation and heat transfer equations, while the convergence criteria, namely the RMS of all equation residuals, is set to 10^{-5}.

The following tables summarize the initial and boundary conditions, according to the specific domain.

Table 4.2 Initial conditions

Domain	Temperature	Other characteristics
Air	23 °C	velocity from the steady case
PCM	23 °C	
Aluminum holding	23 °C	

Table 4.3 Boundary conditions

Domain	Temperature	Other characteristics
Glazing	as seen in figure 4.6	radiation intensity: 318 W/m
inlet	linear variation 23–24°C	velocity: 0.001 m/s
opening	linear variation 23–24°C	relative pressure: 0 Pa
top, bottom, right wall	linear variation 23–24°C	
all other walls	adiabatic	

4.1.3 Results and discussion

The basic aim is to develop a numerical tool, able to reproduce the phenomena, which are observed during a complex case of heat transfer. As already mentioned, this case is suitable to validate a numerical approach of this kind. A comparison of the temperature evolution, at the position marked by the yellow cross in figure 4.3, between the simulation and the experimental results in [35], is shown in figure 4.7.

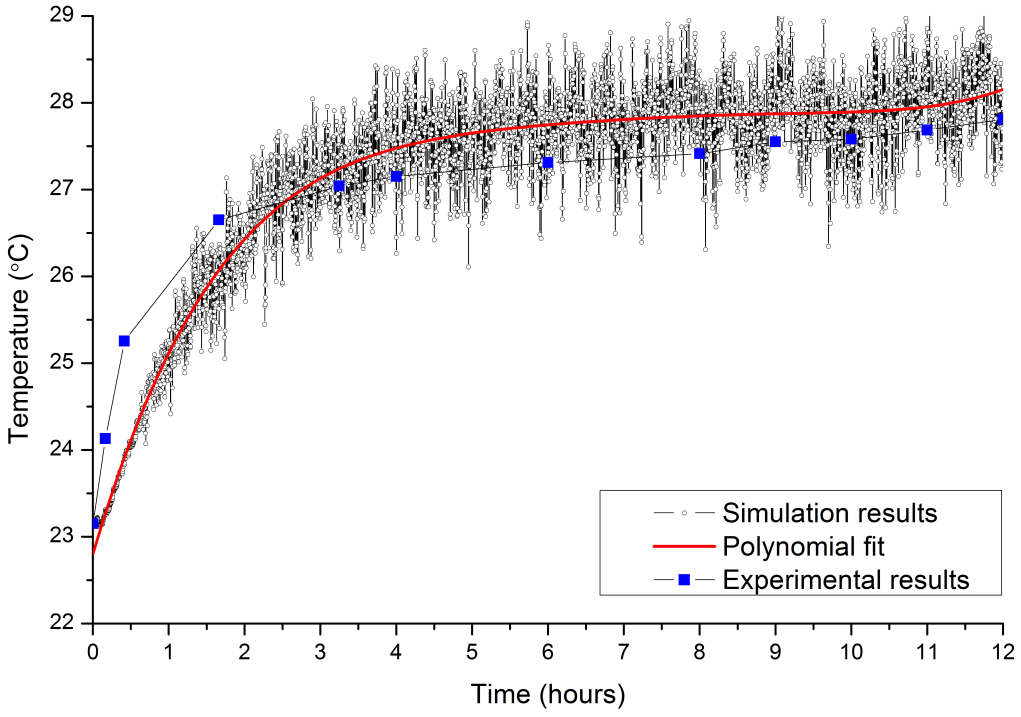

Figure 4.7 Temperature evolution at a distance 5 cm from the blind

The first thing to notice, is the fluctuation of the temperature values throughout the whole duration of the simulation. This can be caused by the import of fresh air from the inlet, which has a temperature lower than the fluid in the specific location. Also, the convergence is very unsteady, fact that can lead to errors in the calculations. Furthermore, the Monte Carlo model is not sufficiently studied. Therefore, an uncertainty in our method is present. Nevertheless, the trend, which is represented by a polynomial fitting of fifth order, shows an acceptable agreement to the actual results. In both simulation and experiment, two characteristic regions exist: i) a sharp increase of the temperature the first 2 hours, and ii) a milder, almost at steady rate increase in the remaining duration.

Regarding the first region, an explanation on this rapidly temperature growth can be the similar trend of the glazing temperature. Also, the temperature is clearly underestimated in the simulations. This fact can be explained, when we consider the absence of heat dumping to the environment (no modeling of the wall and window heat losses). In the experiment, the PCM reaches the melting point after two hours, as seen in figure 4.8. Therefore no latent heat is stored until that point. In the simulation the melting is completed within less than an hour, having stored all the latent heat possible, thus, delaying the heating of the chamber. Additional factors can be:

i. that the thermal conductivity can be adjusted more accurately,
ii. the introduction of fresh air in the system that is colder than in the specific area, and
iii. the two dimension approach, whereas the real case has to be studied in three dimensions for more accurate results.

After the second hour, the temperature in the experiment rises almost at a steady rate with time. This is justified by the fact that, the PCM starts to melt and store heat. The numerical model gradually overestimates the temperature increment. Having already stored all the latent heat possible, the PCM system has a specific heat capacity of 2200 J/kgK. This value can be higher, considering the contribution of the white fabric and the hollow polycarbonate. A more accurate modeling of the specific heat capacity will lead to a higher amount of stored energy, and thus, lower temperature.

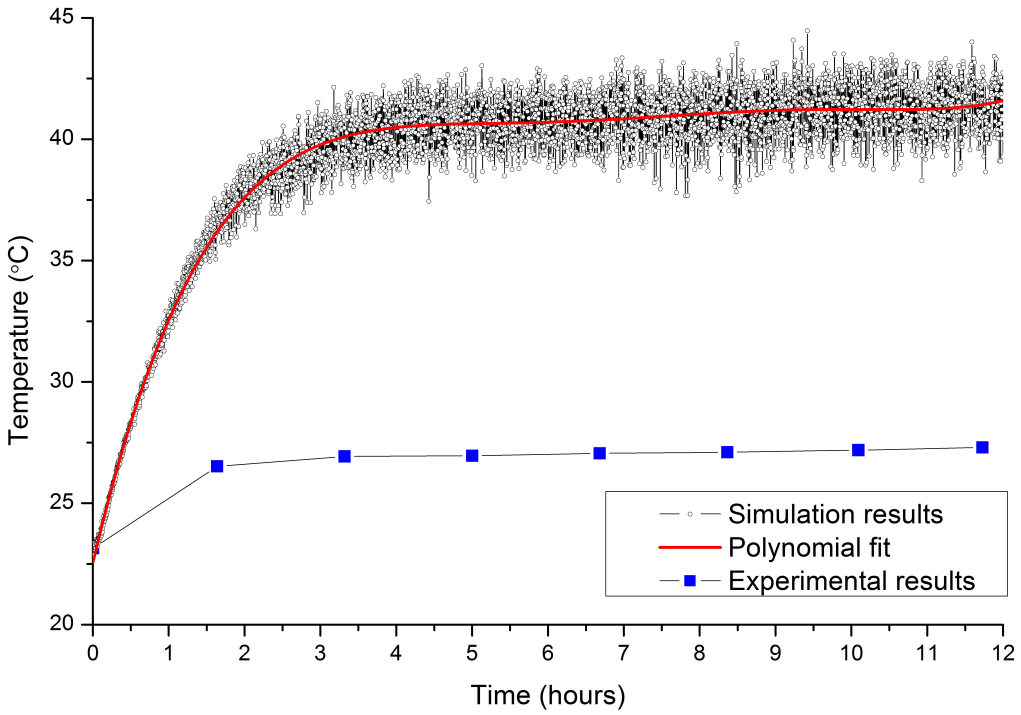

Figure 4.8 Temperature evolution at the inner side of the PCM blind

Further on, the evolution of the temperature field during the simulation is presented in figures 4.9. In figures 4.10 and 4.11 the temperature and flow field are illustrated for the end of the simulation.

Notably, the temperature continuously rises to very high values between the blind and the glazing. Especially the temperature at the blind reaches 52.5 °C, figures 4.9(e), 4.9(f) and 4.10. This is natural to happen, as the entire amount of heat is trapped in this area. Nevertheless, the ambient temperature behind the blind has lower, almost, homogeneous temperature. At the end of the simulation it reaches 27 °C. The energy storing capability of the PCM blind has worked in favor of the thermal protection of the rest part of the room. This is the most important fact, when choosing to install this type of applications. In addition, a closer look can reveal that the upper region of the chamber is hotter than the lower, complying with the buoyancy effect.

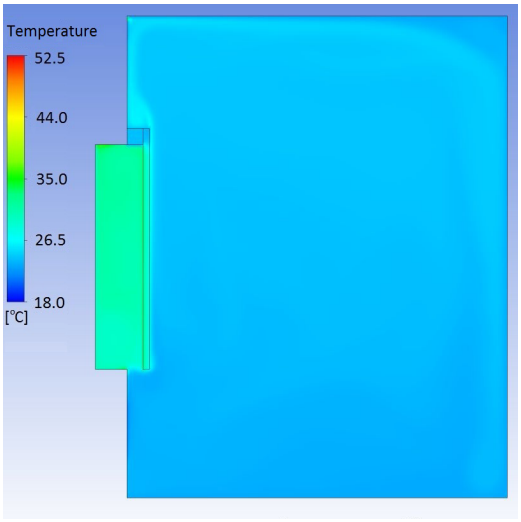

(a) 0.5 hours

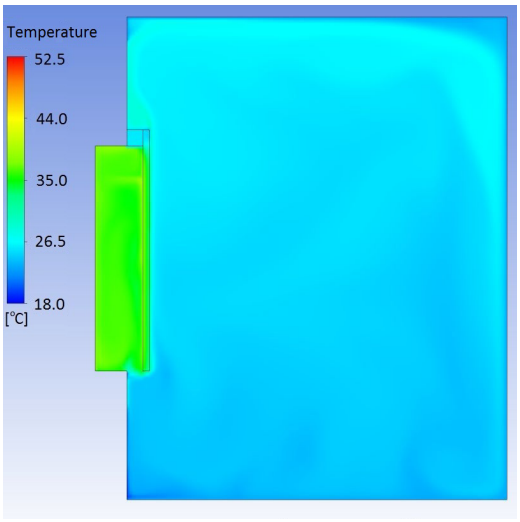

(b) 1 hour

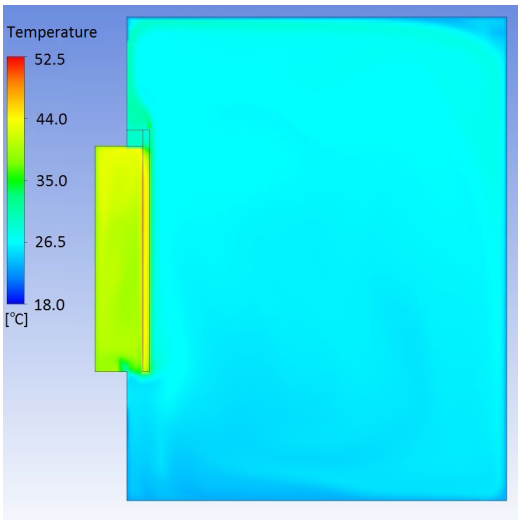

(c) 2 hours

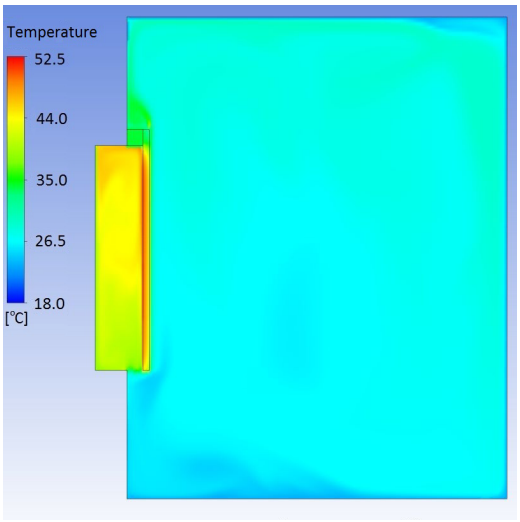

(d) 4 hours

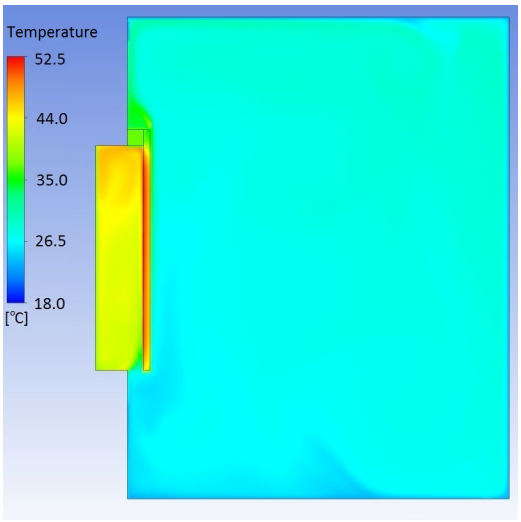

(e) 8 hours

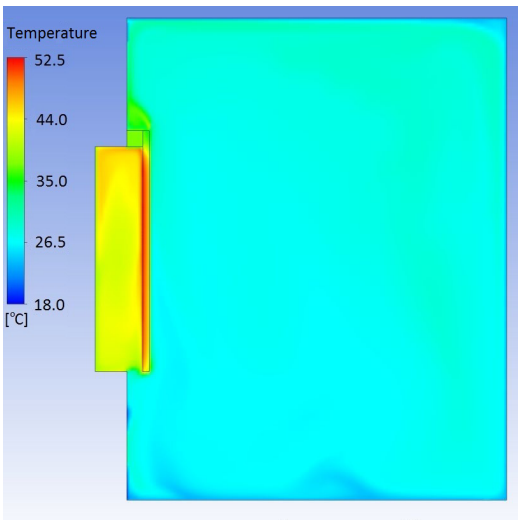

(f) 10 hours

Figure 4.9 Evolution of temperature field during the simulation

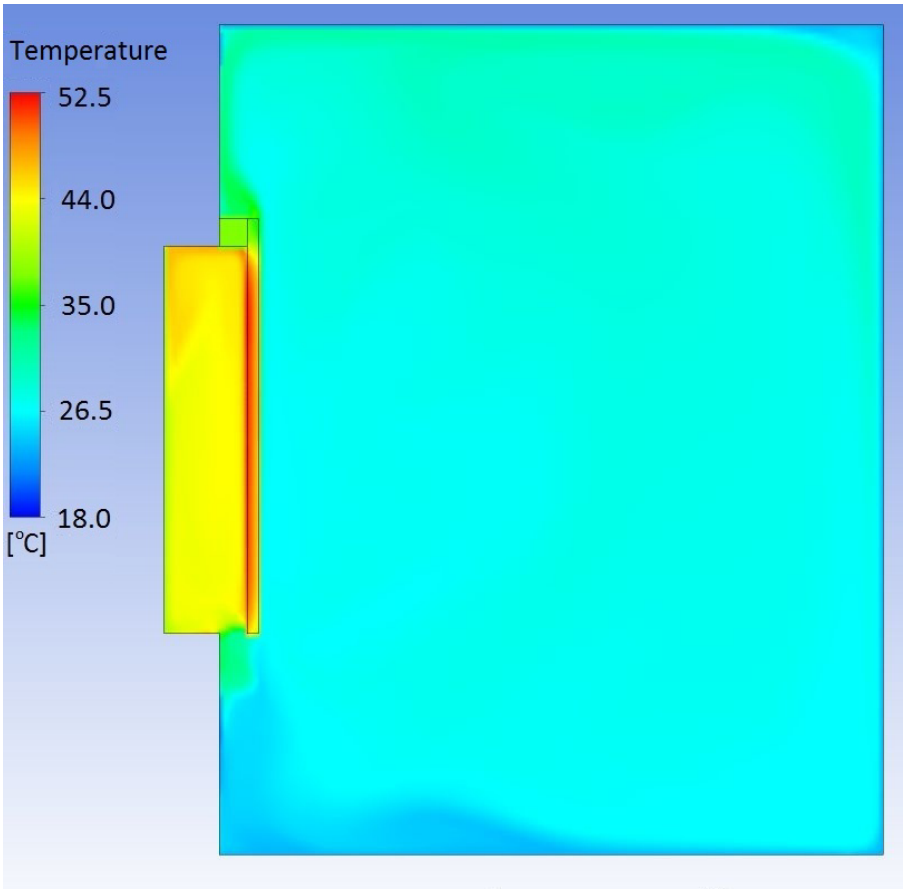

Figure 4.10 Temperature field at the end of the simulation (12 hours)

Figure 4.11 illustrates the flow currents. The complicated behaviour of the flow is evident. Two main regions of recirculation can be observed: one left and one right of the blind. As expected, the velocity is bigger along the side of the blind, driving the warmer air to the upper areas. It is noted that in the left region an increase in velocity is limited due to the smaller area. The highest velocity is lower than $0.7m/s$. Combined with the small lengths this velocity is observed, leads to the calculation of a Reynolds number far smaller than 5×10^5 (almost 7000). Therefore, the assumption of laminar flow is considered valid.

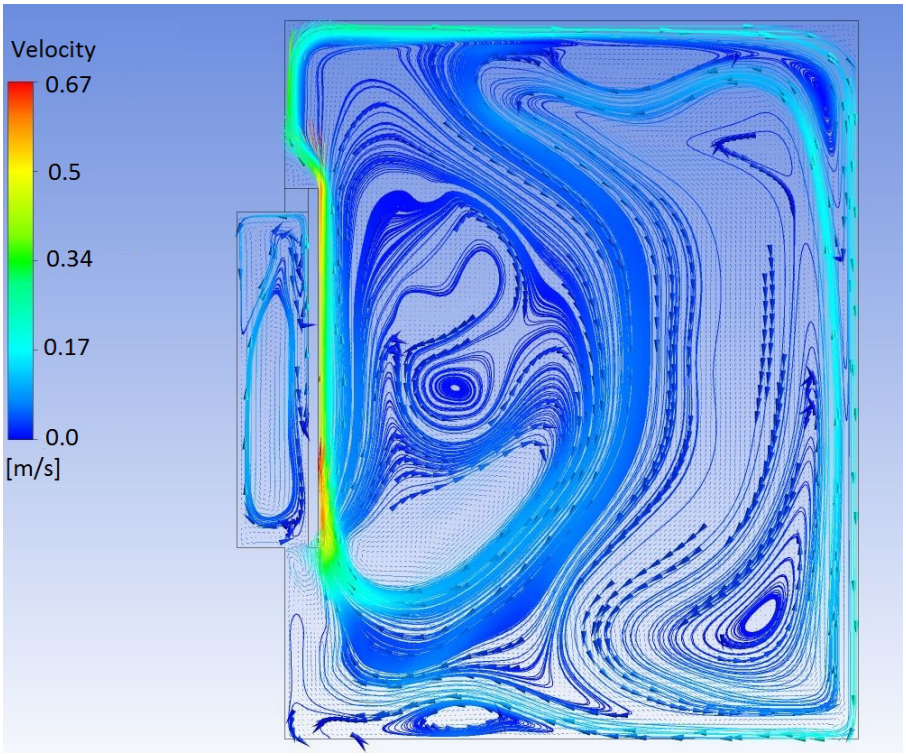

Figure 4.11 Velocity field at the end of the simulation (12 hours)

Concluding this part, a major disadvantage of the method is not including the heat transfer to an exterior colder environment. In other cases, this would lead to severe errors. Nevertheless, the temperature inside the chamber, or rather inside the area in which acceptable thermal conditions are needed, is captured well.

This is a consequence of the successful modeling of the heat, that can be stored from the specific PCM application. This allowed a good agreement to the experimental values. The most significant steps, which led to capturing these very complex phenomena of radiation, natural convection and overall heat transfer are highlighted:

i. implementation of suitable physical principles and the effective heat capacity method, and

ii. combination of a refined good quality mesh with a small time-step.

As a last comment, the actual computation cost of this simulation is presented. In a 64-bit system, with an i7-3770 Intel(R) Core(TM) at 3.4 GHz processor, a parallel running in 4 cores, using 700 MB of RAM, required 3 days and 20 hours to finish. More nodes or smaller time step can be implemented to obtain accuracy, but will lead to a higher cost. This reveals how important is the part of modeling, before continuing to the actual simulations.

4.2 Installation of a phase change material slats on existing walls

4.2.1 Physical properties and geometry configuration

The objective is to prevent excessive heating on the surface of the wall in the summer, and minimize the heat transfer to the outside of the building in the winter. Therefore, the installation of a PCM building application on a wall is investigated.

This application, which will be refereed to as PCM slats from here on, is illustrated in figure 4.12. It consists of an installation support framework and five individual parts. Each part integrates two components: a layer of an insulation material, and the PCM contained in an aluminum holding. A rotational system is also embedded to each PCM slats as well. This gives the potential to the system to rotate from position 1. to position 4. as seen in the illustration. Figure 4.13 shows the geometrical dimensions in each PCM slats position. Note that, this figure gives a simplified representation of the actual PCM application. Also, the interior does no indicate the inside of the building, but rather the innermost air domain. The horizontal cavity is formed from the building wall, the top and bottom wall of the support framework of the application, and has 200 mm length and 560 mm height.

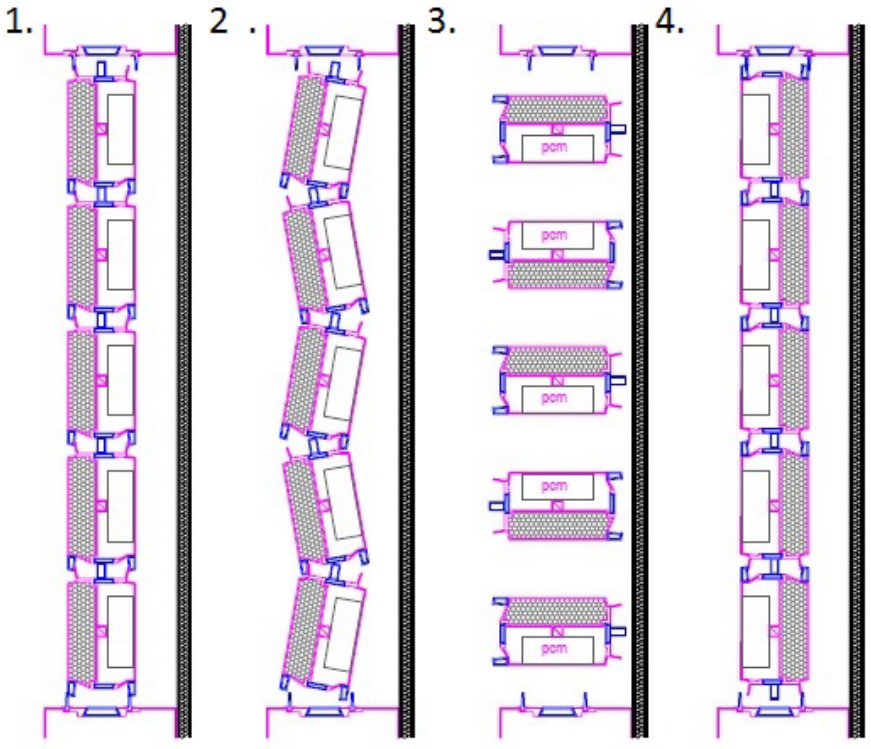

Figure 4.12 Configuration of the PCM slats

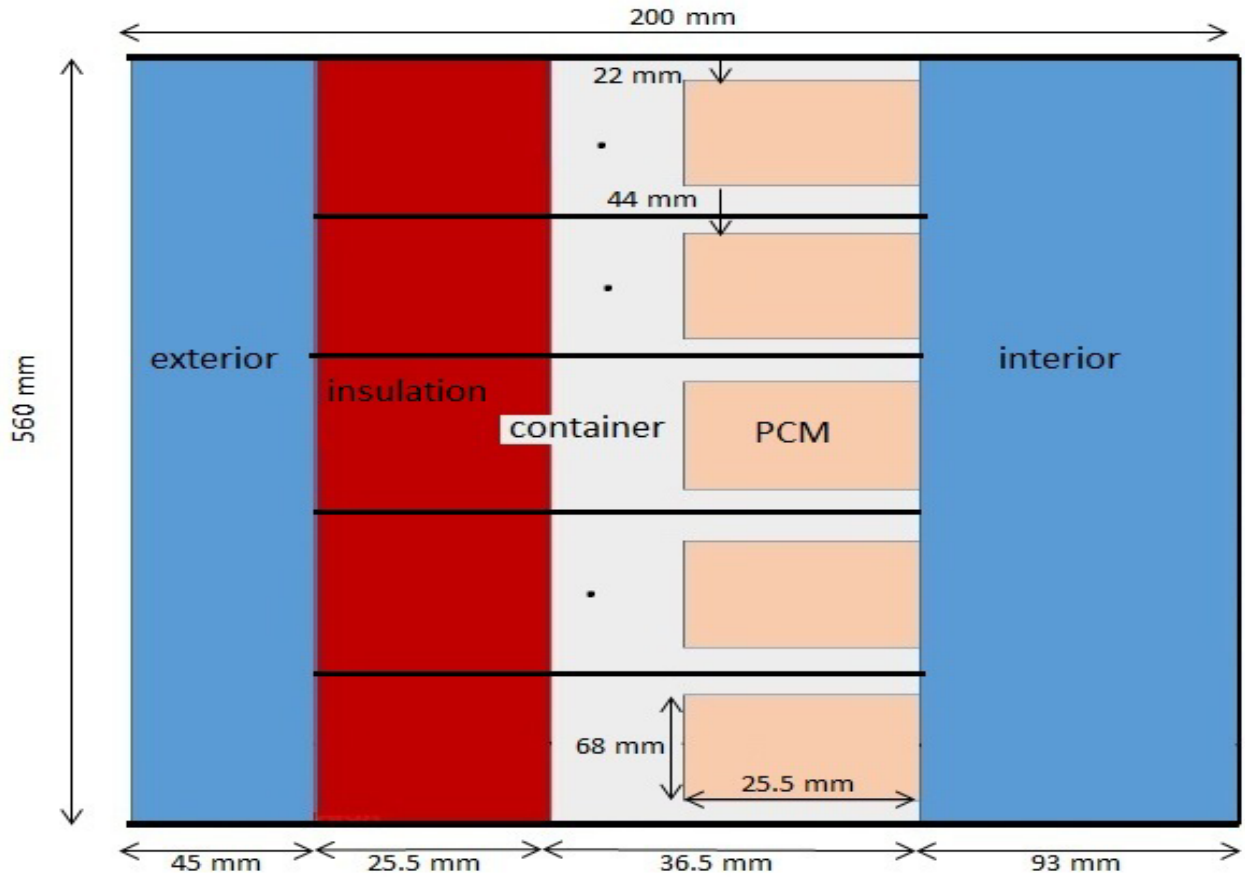

(a) Geometry of first position of PCM slats

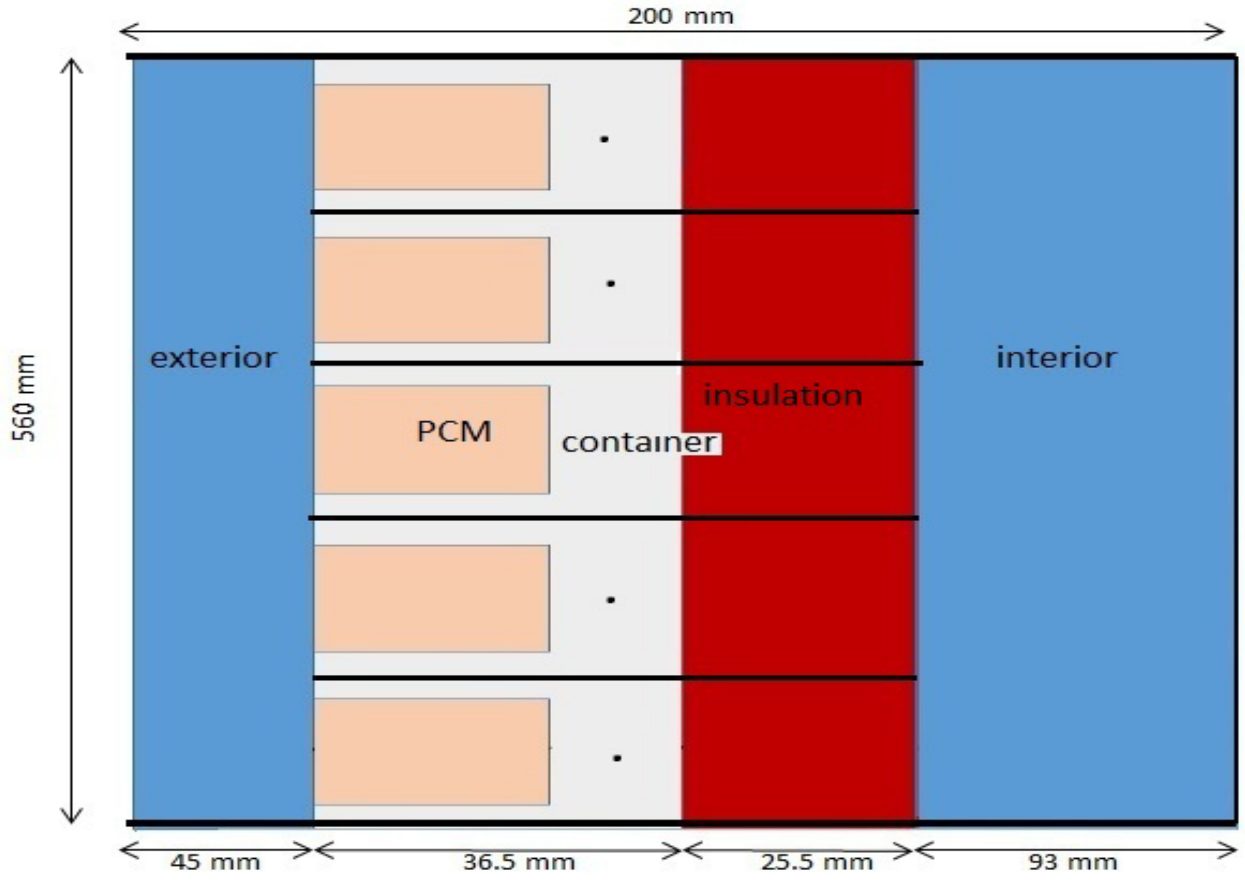

(b) Geometry of second state of configuration

Figure 4.13 Geometry characteristics of the PCM slats in two configurations

Next, the properties of each material are presented. The melting enthalpy and the melting range of the PCM, are 170 kJ/kg and 19.5–22.5 °C, respectively. The density is 1530 kg/m^3, the thermal conductivity is 0.54 W/mK, and the specific heat capacity 2200 J/kgK. The container of the PCM is mainly build from aluminum, with density 2702 kg/m^3, thermal conductivity 237 W/mK, and specific heat capacity 903 J/kgK. The application is, also, incorporating an insulation layer of polyurethane foam. Its density is 55 kg/m^3, thermal conductivity is 0.027 W/mK, and the specific heat capacity 1210 J/kgK. We sum up there characteristics in table 4.4. In addition, we treat the specific heat capacity of the PCM similar to the first case with equation 4.2, as shown in figure 4.14. In addition, the absorption coefficient for the insulation layer is 0.08, and 0.98 for the aluminum-PCM component.

Table 4.4 Properties of materials consisting the PCM slat

	PCM	Aluminum	Polyurethane foam
density (kg/m^3)	1530	2702	55
thermal conductivity (W/mK)	0.54	237	0.027
specific heat capacity (J/kgK)	figure 4.14	903	1210

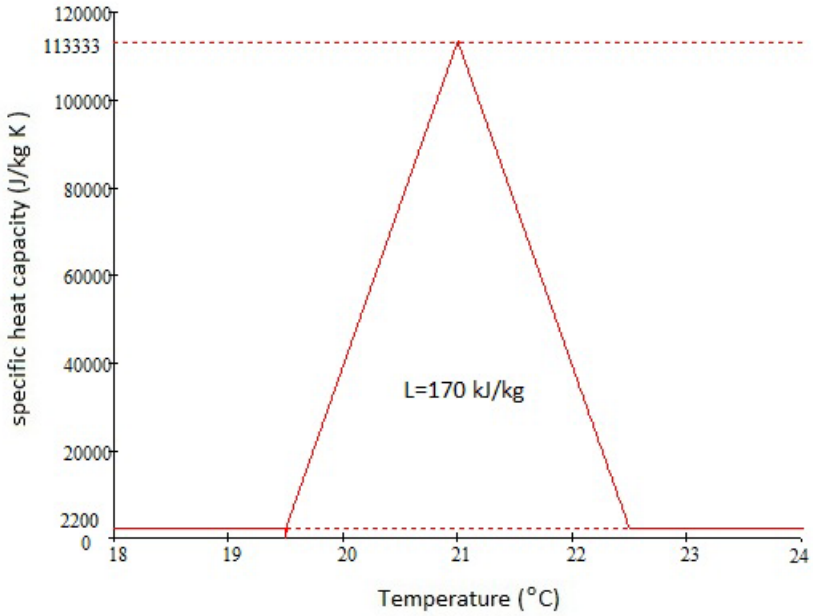

Figure 4.14 Heat transfer coefficient of PCM

$$c_p(T) = \begin{cases} 2200 & ,T < 19.5°C \\ 2200 + 74088.66\,(T - 19.5) & ,19.5 \geq T \geq 21°C \\ 2200 - 74088.66\,(T - 22.5) & ,21 \geq T \geq 22.5°C \\ 2200 & ,T > 22.5°C \end{cases} \tag{4.2}$$

Describing the other aspects of the case studied, the top and the bottom walls of the framework are adiabatic, while the right is the wall of an existing building. In the building, the ambient temperature is 20 °C, while the heat transfer coefficient is 0.5024 W/m^2K. The PCM slat is installed at a distance of 93 mm from the wall, as shown in figure 13(a). When the system rotates the insulation arrives to the same position, figure 13(b). From here on, we will denote the first position with the letter a and the second with b.

4.2.2 Numerical modeling

First of all, the grid is created in order enhance accuracy. Hence, a homogeneous discretizaton of 2.5 mm for every element is chosen. This leads to a total number of 18000 rectangular cells. The grid is illustrated in figure 4.15 for the first configuration. In addition, 40000 iterations are imposed for every case, with a convergence criteria target of 10^{-4}. This very well refined mesh combined with the amount of iterations, shall be able to capture the natural convection accurately.

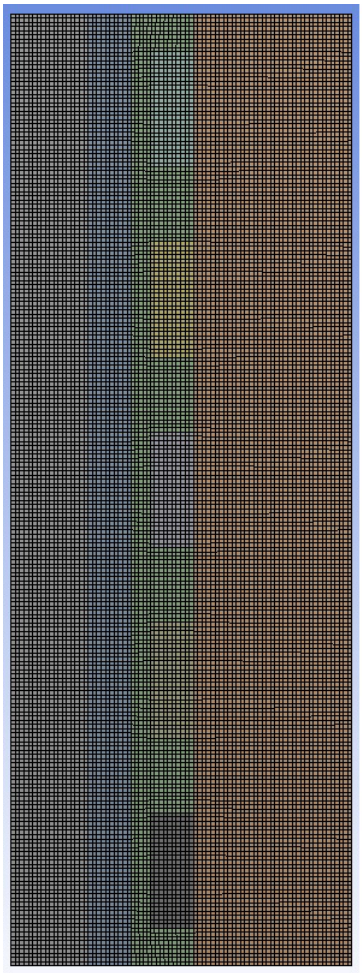

Figure 4.15 Numerical grid for the first position of the PCM slats

We consider two cases. In the first, denoted as *1*, the temperature of the environment is 26

°C, and the radiation emitting from the exterior domain normal to the slat has an intensity of 445 W/m^2. In the second case (*2*), these properties have the values 15 °C and 1300 W/m^2, respectively. These values correspond to the meteorological conditions observed in Sevilla (Spain) at 14:00, on the 21st of July and 21st of March, respectively.

These properties are used as initial values to our simulations. In addition, a vertical velocity of 0.0001 m/s is set, and the temperature in all domains are the same as the exterior. Furthermore, in order to evaluate the impact of the PCM slats, an third set of simulations is needed to predict the temperature in a state, where no installation of the PCM has taken place for the two cases.

In each case, both exterior and interior domain are modeled as air ideal gas. The buoyancy effect and a laminar model are enabled for both domains. The left side is treated as an opening with relative pressure of 0 Pa. The remaining physical characteristics and boundary conditions are described in the previous section. As a last note, in the cases where no PCM slat was involved, the same grid is used, but only an exterior domain is simulated.

Table 4.5 summarizes the simulation according to positions of the PCM slats, if applicable, and the ambient conditions.

Table 4.5 Simulation cases for PCM slats

simulation	PCM slat position	Temperature °C	Radiation W/m^2
1	no slats	26	445
1a	position 1	26	445
1b	position 2	26	445
2	no slats	15	1300
2a	position 1	15	1300
2b	position 2	15	1300

In order to capture the beneficial impact of PCM on the energy consumption, transient simulations should take place. This kind of simulations poses a challenge on the set up, adjusting the timestep and the boundary conditions. In this case, time limits towards the submission of this thesis, have played a decisive role of not carrying out the specific simulations.

4.2.3 Results for the first case

First, the temperature and the heat fluxes along the wall, for all cases *1* are compared, in figures 4.16 and 4.17, respectively. In the specific case, the aim of the PCM slats installation is to create favorable conditions, for a moderate increase in the temperature on the wall.

In the steady state where no application is installed, the highest temperature, 83 °C, appears at the top of the wall. This is to be expected due to the natural convection. The mean

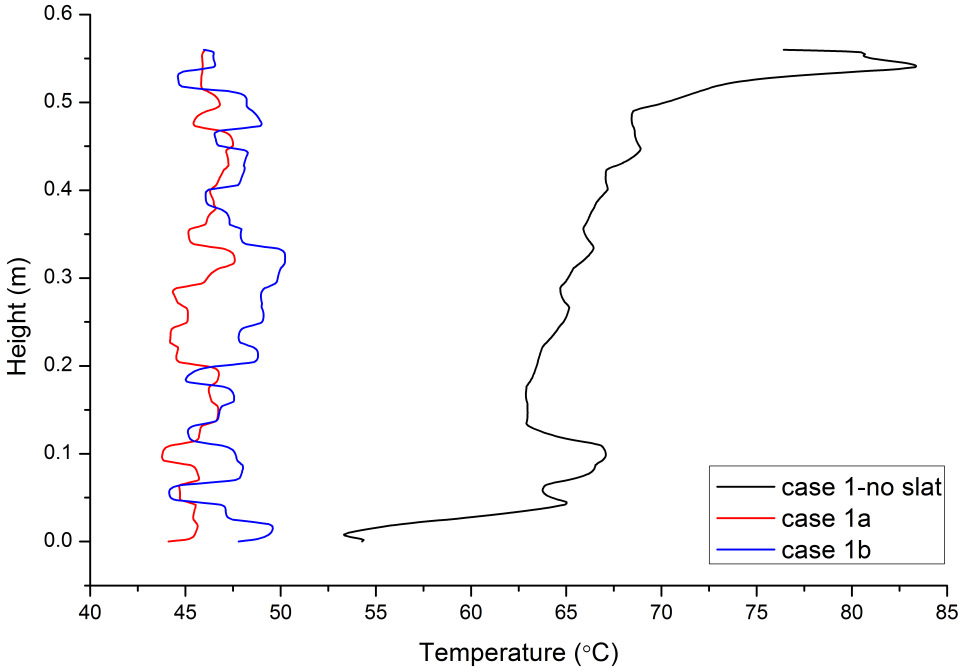

Figure 4.16 Prediction of temperature along the wall for cases *1*

temperature of the wall is around 65 °C. On the other hand, for cases *1a* and *1b* the temperature is kept to around 46 °C. In addition, the heat fluxes have considerable smaller magnitude, almost two times smaller. This fact indicates that, less heat is transferred through the wall to the interior of the building. The negative sign is present, due to he fact that the interior of the building is colder that the environment. Furthermore, for both temperature and heat flux, a more uniform behaviour, compared to the same properties for the "naked" wall is observed.

These are the most important outcomes of these simulations. The PCM blind has a positive effect in the thermal protection of the building, although a comparison should be held with slats without PCM, in order to see to what extend this impact is more advantageous. The fact that, almost the same temperature is evident for both PCM slats configurations, is expected. This emerges from the fact that, we investigate their behaviour in a steady state. It would be interesting to see the evolution of the temperature in time.

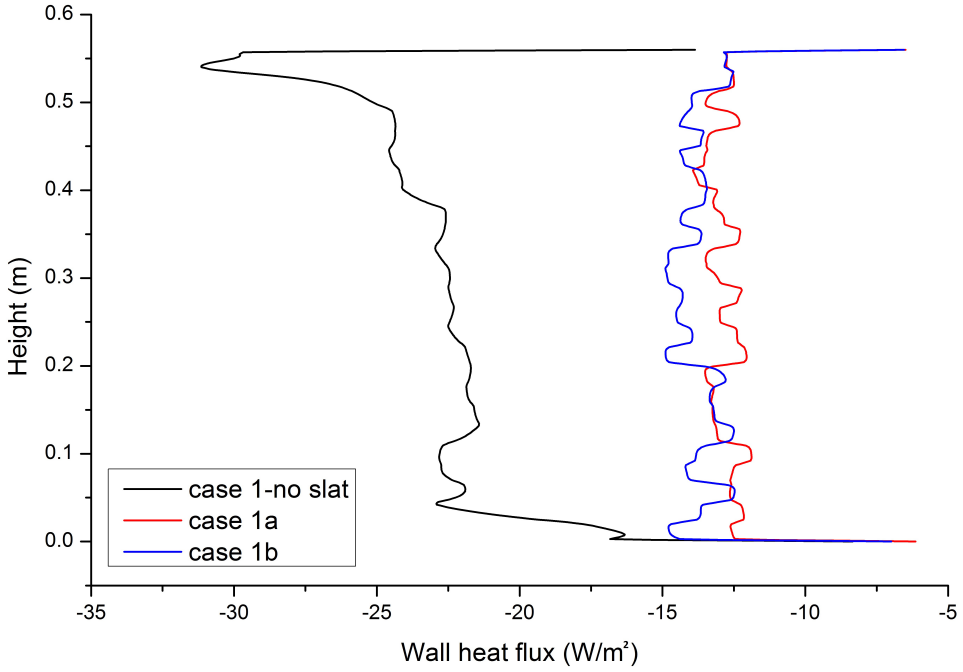

Figure 4.17 Prediction of heat flux along the wall for cases *1*

Further on, we demonstrate the temperature and the flow field in the cavity, when no PCM system is installed, figure 4.18. Despite the fact that the temperature on the wall is very high, the rest of the domain remains in a temperature range of 27 to 32 °C. The high temperature at the bottom right of the domain is a result of the recirculation, which occurred in that area. We, also, note that the highest velocity is 0.6 m/s near the top of the opening and the anticlockwise direction of the recirculation is as the hot air rises and drags the air coming from the outside along with it.

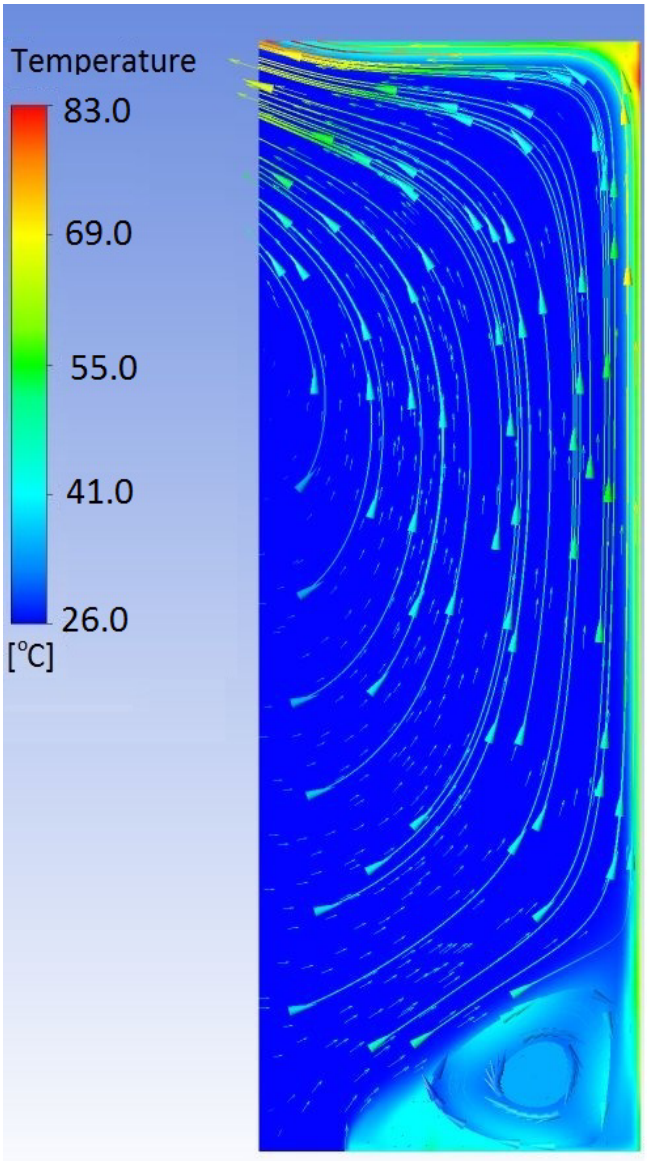

Figure 4.18 Prediction of the temperature field and streamlines for case *1* with no PCM slats

Next, the two positions of the system are ompared to each other, case *1a* and *1b* in figures 4.19(a) and 4.19(b). Note that the initial temperature in the environment is 26 °C. This means that the PCM is already melted, thus, has already stored the amount of latent heat possible.

The main difference is the temperature of the PCM. In case *1a* the PCM reaches 48 °C, whereas in case *1b* 64 °C. However, this difference can lead to no assumption on which state is preferable to adopt, in order to help the interior of the building to preserve the desirable temperature, within minimum energy consumption of the HVAC system.

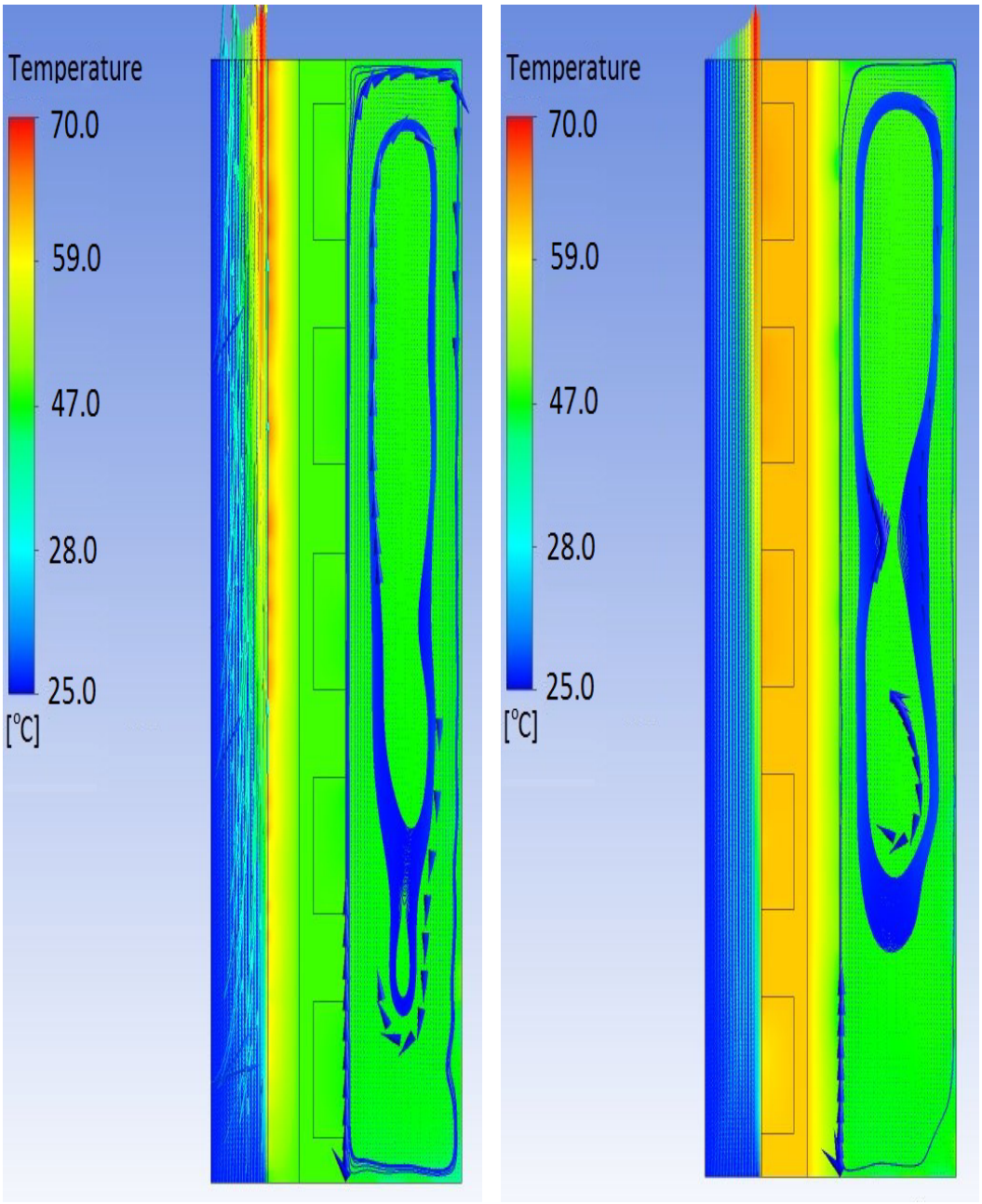

(a) Case *1a* (b) Case *1b*

Figure 4.19 Prediction of the temperature field and streamlines for case *1* with PCM slats

4.2.4 Results for the second case

In this case, the system should help to prevent the heat loss from the building. This cannot be seen from the steady state. Even though the ambient temperature is low, 15 °C, the radiation is so large that leads to nonphysical temperature rise for a winter day. This case is equivalent to a cold summer day with high radiation levels.

Similar aspects for this case as for the previous one are discussed here. The results for the temperature and the heat fluxes on the wall can be seen in figures 4.20 and 4.21. The maximum temperature is observed in the same position as before, but due to the larger radiation magnitude the temperature reaches 147 °C. The average value on the wall is lower, though, rising to 112 °C. Also, the heat flux is rising with the rising height of the wall, reaching 65 W/m^2. Both temperature and heat flux present a highly volatile behaviour. On the other hand, the PCM slats preserve the temperate and heat fluxes in low values. In addition, the same steady behaviour is observed as in case *1* for these two properties.

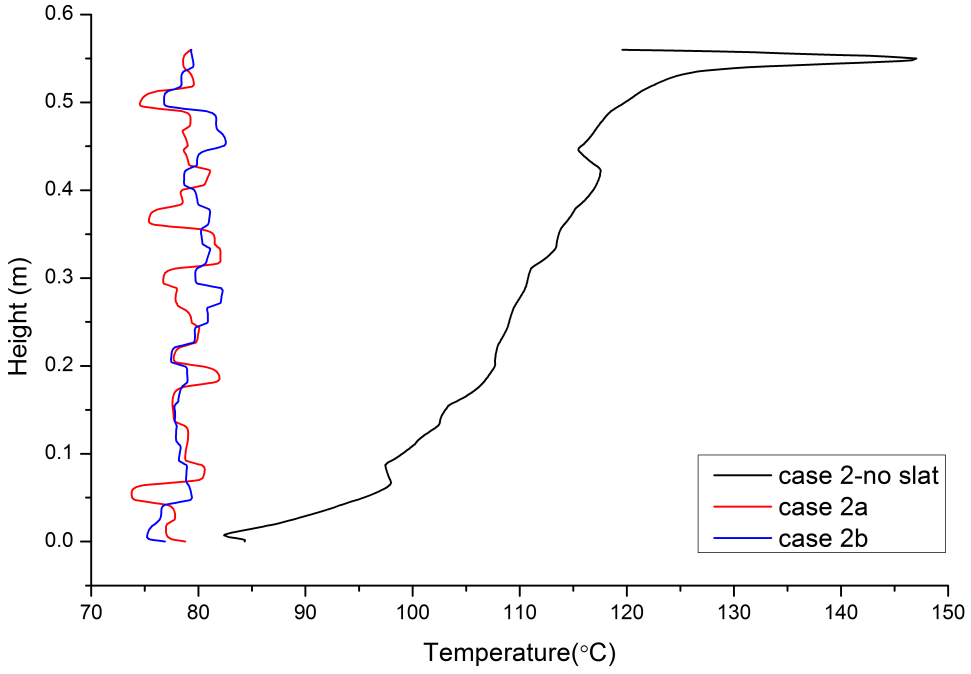

Figure 4.20 Prediction of the temperature along the wall for case *2*

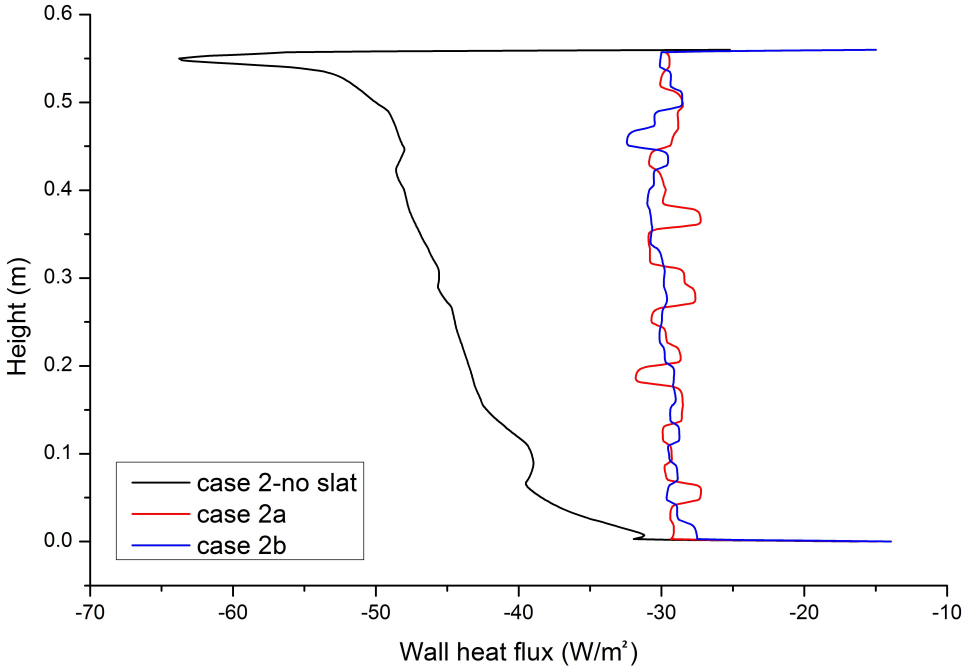

Figure 4.21 Prediction of the heat flux along the wall for case *2*

The field characteristics are presented next. First, the cavity without any PCM slats is showed in figure 4.22. The temperature remains at 15 °C, almost in the whole domain. The maximum velocity is not very different, 0.82 m/s to the first case either. However, the recirculation shows a contrasting behaviour comparing to case *1*, probably due to the fact that cold air is entering the domain.

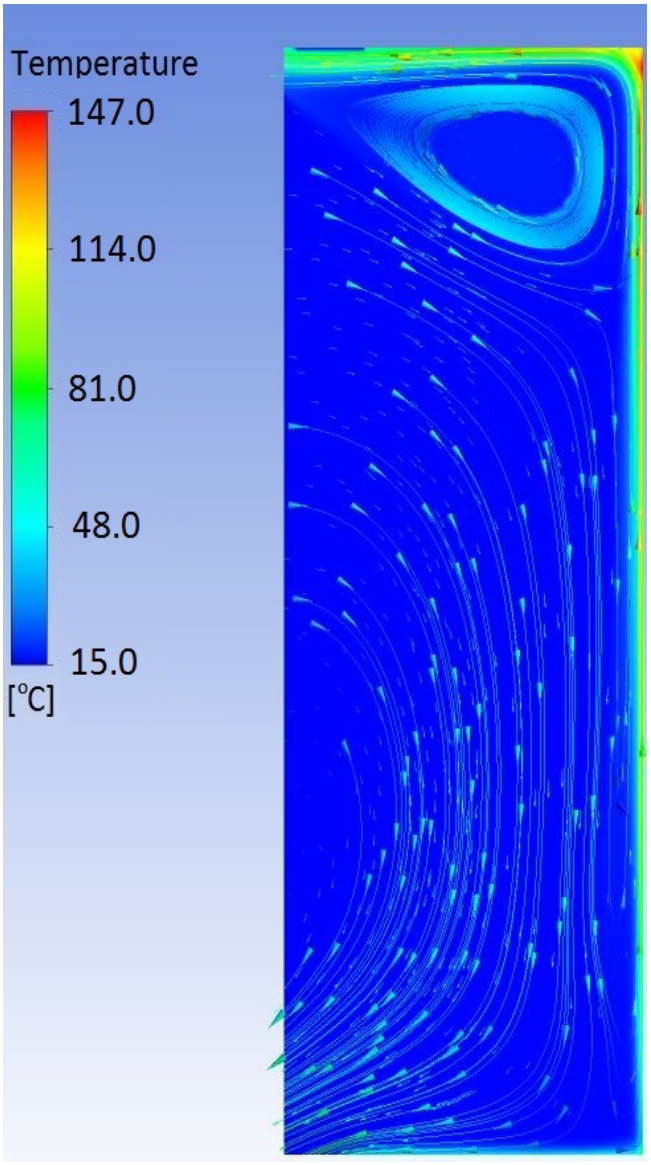

Figure 4.22 Prediction of the temperature field and streamlines for case *2* with no PCM slats

It is more interesting to compare the different configuration states, figure 4.23(a) and 4.23(b). The resulting temperature in the back wall is almost the same, 82 and 78 °C respectively. The important fact is that, the PCM in the second case has heated a lot more. This indicates that, during the night, a higher amount of energy can be provided to the building, after the rotation of the slats, from position *2* to position *1*. However, this fact is not clear in these simulations. Transient simulations can, possibly, verify this assumption. Note that, the velocity and recirculation behaviour is the same for both states.

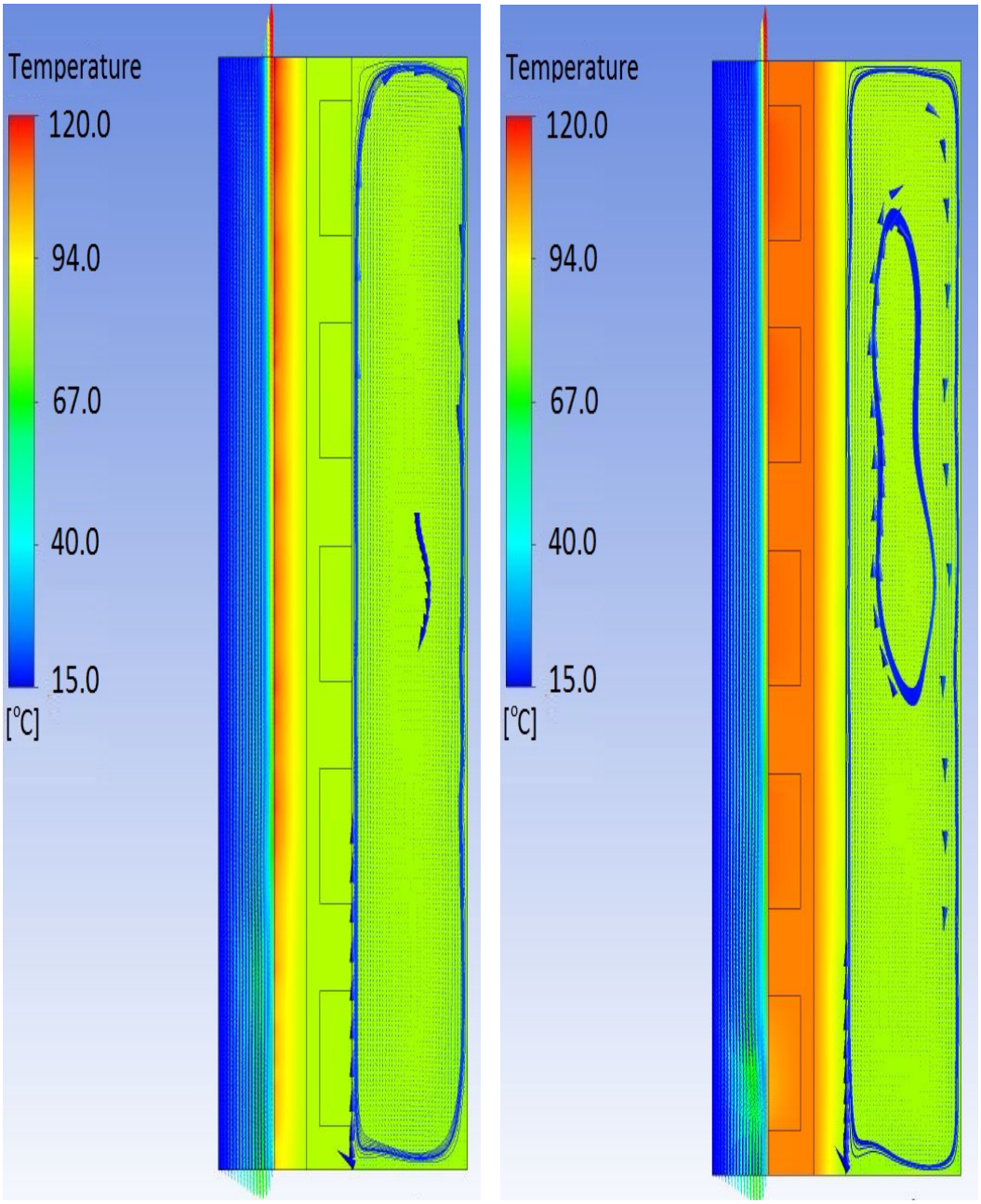

(a) Case *2a* (b) Case *2b*

Figure 4.23 Prediction of the temperature field and streamlines for case *2* with PCM slats

4.3 Conclusions and discussion on the simulations

In both cases, heat transfer through building elements, in which a PCM is integrated, was simulated. The heating is caused by an external radiation source. Due to the buoyancy effect, natural convection has developed. The temperature and the flow field is illustrated, and a complex behaviour in each system is observed. Also, both simulation were conducted in two dimensional domains.

In particular, the first case acted as a validation tool to the numerical modeling. The temperature growth inside the chamber during the evolution of time was reproduced. In this scope, the results gave a satisfactory image comparing to the experimental values. This fact led to claim the suitability of the effective heat capacity method, the grid refinement and the time step.

Nevertheless, it is important to note, that the method has a weakness. Two factors were not taken into account: the exterior environment, which temperature remained at 25 °C [35], and the possibility of heat transfer from the chamber through the window. Hence, a great amount of heat was trapped between the window and the blind, and an excessive amount of sensible heat was stored in the PCM blind. This issue can be treated by assigning a parameter, equivalent to the U-value of the window.

On the other hand, this problem did not affected the results in the second case. In this situation, no windows exist prior to the building walls. The outcome of the second part of simulations, verified the beneficial impact on thermal protection during the summer period. Regarding the winter period, the study showed a favorable position of the PCM facing the outer direction to store as much heat possible and return it to the building after rotation during the cooling process. To validate this estimation the steady state simulations need to advance to transient simulations.

To sum up, the most important feature assessed is the capability of heat storing in a PCM system. Adopting the effective heat capacity proved to be quite efficient. Also, the fact that the only prerequisites to apply it are the melting enthalpy and the melting temperature range, makes the method even more appealing. In addition, two dimension modeling provide accuracy, as well as, moderate computational cost. Finally, transient simulation seems to be necessary to support more valid conclusions.

5 Overall remarks and future work

The motivation behind this thesis, was to address the energy efficiency in buildings. A promising approach is using PCM to increase the efficiency of thermal energy systems. Nevertheless, this solution is not trivial. Careful consideration of all the contributing features will lead to the utmost exploit of their characteristics.

Also, this work highlights the complicated behaviour of fluid dynamics in a heat transfer case. Computational fluid dynamics can contribute towards the designing and assessment of building applications. The method developed in this work, is suitable in this scope, although some of its aspects, mentioned in the previous chapter, can be modified to lead to a better performance. Perhaps, it should be stated once more, the convenience and accuracy of the effective heat capacity method.

Further simulations are recommended, where instead of the PCM, a conventional material can be implemented. This can show to what extend the integration of PCM is beneficial. In addition, the designing process can be enhanced with transient simulations. They could, possibly, show an acceptable estimation of the amount of heat, that the PCM can store in a period of a whole day. Even more, cases where the configuration of the PCM slats can change during the evolution of the temperature, should be considered as the final simulation goal.

References

[1] International Energy Agency. http://www.iea.org/aboutus/faqs/renewableenergy/. Retrieved January 2014.

[2] Luís M. A. Bettencourt, Jessika E. Trancik, and Jasleen Kaur. Determinants of the pace of global innovation in energy technologies. *PLoS ONE, 8(10):e67864, 10*, 2013.

[3] THE EUROPEAN ECONOMIC REPORT FROM THE COMMISSION TO THE EUROPEAN PARLIAMENT, THE COUNCIL, SOCIAL COMMITTEE, and THE COMMITTEE OF THE REGIONS Renewable energy progress report. 2013.

[4] European environment agency. Final energy consumption by sector (CSI 027/ENER 016) Assessment published Feb 2013.

[5] Belén Zalba, José M. Marín, Luisa F. Cabeza, and Harald Mehling. Review on thermal energy storage with phase change: materials, heat transfer analysis and applications. *Applied Thermal Engineering 23 (2003) 251–283*, 2003.

[6] Atul Sharma, V.V. Tyagi, C.R. Chen, and D. Buddhi. Review on thermal energy storage with phase change materials and applications. *Renewable and Sustainable Energy Reviews 13 (2009) 318–345*, 2009.

[7] IEA-ETSAP and IRENA Technology-Policy Brief E17. January 2013.

[8] INSIGHTS FOR POLICY MAKERS Technology Brief IEA-ETSAP Thermal Energy Storage and IRENA Technology Brief E17. January 2013.

[9] John F. Wendt (editor). *Computational Fluid Dynamics, An Introduction*. Springer, Third Edition, 2009.

[10] Mohammed M. Farid, Amar M. Khudhair, Siddique Ali K. Razack, and Said Al-Hallaj. A review on phase change energy storage: materials and applications. *Energy Conversion and Management 45 (2004) 1597–1615*, 2004.

[11] L.F. Cabeza, A. Castell, C. Barrenechea, A. de Graciaa, and A.I. Fernández. Materials used as pcm in thermal energy storage in buildings: A review. *Renewable and Sustainable Energy Reviews 15 (2011) 1675–1695*, 2011.

[12] Frédéric Kuznik, Damien David, Kevyn Johannes, and Jean-Jacques Roux. A review on phase change materials integrated in building walls. *Renewable and Sustainable Energy Reviews 15 (2011) 379–391*, 2011.

[13] Adem Ugurlun and Cihan Gocko. A review on thermal energy storage systems with phase change materials in vehicles. *Electronic Journal of Vocational Colleges*, 2012.

[14] D. Zhou, C.Y. Zhao, and Y. Tian. Review on thermal energy storage with phase change materials and applications. *Applied Energy 92 (2012) 593–605*, 2012.

[15] Halime Ö. Paksoy. *Thermal Energy Storage for Sustainable Energy Consumption*. Springer, P.O. Box 17, 3300 AA Dordrecht, The Netherlands, 2007.

[16] H Mehling and L.F. Cabeza. *Heat and cold storage with PCM; An up to date introduction into basics and applications*. Springer, 2008.

[17] Dionysios I. Kolaitis, Eleni K. Asimakopoulou, and Maria A. Founti. Gypsum plasterboards enhanced with phase change materials: A fire safety assessment using experimental and computational techniques. *MATEC Web of Conferences 9, 06002*, 2013.

[18] Cemil Alkan, Eva Günther, Stefan Hiebler, Ömer Faruk Ensari, and Derya Kahraman. Polyethylene glycol-sugar composites as shape stabilized phase change materials for thermal energy storage. *Polymer Composites*, 33(10):1728–1736, 2012.

[19] G. Evola, L. Maletta, and F. Sicurella. A methodology for investigating the effectiveness of pcm wallboards for summer thermal comfort in buildings. *Building and Environment 59 (2013) 517–527*, 2013.

[20] Simone Raoux and Matthias Wuttig. *Phase Change Materials, Science and Applications*. Springer, 2009.

[21] Maha Ahmad, André Bontemps, Hébert Sallée, and Daniel Quenard. Thermal testing and numerical simulation of a prototype cell using light wallboards coupling vacuum isolation panels and phase change material. *Energy and Buildings 38 (2006) 673–681*, 2006.

[22] P. Schossigaa, H.-M. Henning, S. Gschwander, and T. Haussmann. Micro–encapsulatedphase–change materials integratedinto construction materials. *Solar Energy Materials Solar Cells 89 (2005) 297–306*, 2005.

[23] Maha Ahmad, André Bontemps, Hébert Salleé, and Daniel Quenard. Thermal testing and numerical simulation of a prototype cell using light wallboards coupling vacuum isolation panels and phase change material. *Energy and Buildings 38 (2006) 673–681*, 2006.

[24] Lv Shilei, Zhu Neng, and Feng Guohui. Impact of phase change wall room on indoor thermal environment in winter. *Energy and Buildings 38 (2006) 18–24*, 2006.

[25] Luisa F. Cabeza, Cecilia Castellón, Miquel Nogués, Marc Medrano, Ron Leppers, and Oihana Zubillaga. Use of microencapsulated pcm in concrete walls for energy savings. *Energy and Buildings 39 (2007) 113–119*, 2007.

[26] Conrad Voelker, Oliver Kornadt, and Milan Ostry. Temperature reduction due to the application of phase change materials. *Energy and Buildings 40 (2008) 937–944*, 2008.

[27] F. Kuznik, J. Virgone, and J. J. Roux. Energetic efficiency of room wall containing pcm wallboard: A full-scale experimental investigation. *Energy and Buildings 40 (2008) 148–156*, 2008.

[28] F. Kuznik and J. Virgone. Experimental investigation of wallboard containing phase change material: Data for validation of numerical modeling. *Energy and Buildings 41 (2009) 561–570*, 2009.

[29] F. Kuznik and J. Virgone. Experimental assessment of a phase change material for wall building use. *Energy and Buildings 41 (2009) 561–570*, 2009.

[30] Hongim Liu and Hazim B. Awbi. Performance of phase change material boards under natural convection. *Building and Environment 44 (2009) 1788–1793*, 2009.

[31] Ana Vaz Sá, Miguel Azenha, Hipólito de Sousa, and António Samagaio. Thermal enhancement of plastering mortars with phase change materials: Experimental and numerical approach. *Energy and Buildings 49 (2012) 16–27*, 2012.

[32] Pablo Arce, Cecilia Castellón, Albert Castell, and Luisa F. Cabeza. Use of microencapsulated pcm in buildings and the effect of adding awnings. *Energy and Buildings 44 (2012) 88-93*, 2012.

[33] Chun long Zhuang, An zhong Deng, Yong Chen, Sheng bo Li, Hong yu Zhang, and Guo zhi Fan. Validation of veracity on simulating the indoor temperature in pcm light weight building by energyplus.

[34] A. Carbonari, M. De Grassi, C. Di Perna, and P. Principi. Numerical and experimental analyses of pcm containing sandwich panels for prefabricated walls. *Energy and Buildings 38 (2006) 472-483*, 2006.

[35] Helmut Weinlaeder, Werner Koerner, and Michael Heidenfelder. Monitoring results of an interior sun protection system with integrated latent heat storage. *Energy and Buildings 43 (2011) 2468–2475*, 2011.

[36] D. Feldman, D. Banu, and D.W. Hawes. Development and application of organic phase change mixtures in thermal storage gypsum wallboard. *Solar Energy Materials and Solar Cells 36 (1995) 147–157*, 1995.

[37] Zhaolin Gu, Hongjuan Liu, and Yun Li. Thermal energy recovery of air conditioning system- heat recovery system calculation and phase change materials development. *Applied Thermal Engineering 24 (2004) 2511–2526*, 2004.

[38] Lv Shilei, Feng Guohui, Zhu Neng, and Dongyan Li. Experimental study and evaluation of latent heat storage in phase change materials wallboards. *Energy and Buildings 39 (2007) 1088–1091*, 2007.

[39] Chi ming Lai, R.H. Chenb, and Ching-Yao Lin. Heat transfer and thermal storage behaviour of gypsum boards incorporating micro-encapsulated pcm. *Energy and Buildings 42 (2010) 1259–1266*, 2010.

[40] Alvaro de Gracia, Camila Barreneche, Mohammed M. Farid, and Luisa F. Cabeza. New equipment for testing steady and transient thermal performance of multilayered building envelopes with pcm. *Energy and Buildings 43 (2011) 3704–3709*, 2011.

[41] Colas Hasse, Manuel Grenet, André, Bontemps, and Hébert Sallée Rémy Dendievelb. Realization, test and modelling of honeycomb wallboards containing a phase change material. *Energy and Buildings 43 (2011) 232–238*, 2011.

[42] Annabelle Joulin, Zohir Younsi, Laurent Zalewski, Stéphane Lassue, Daniel R. Rousse, and Jean-Paul Cavrot. Experimental and numerical investigation of a phase change material: Thermal-energy storage and release. *Applied Energy 88 (2011) 2454–2462*, 2011.

[43] Manuel Ibáñez, Ana Lázaro, Belén Zalba, and Luisa F. Cabeza. An approach to the simulation of pcms in building applications using trnsys. *Applied Thermal Engineering 25 (2005) 1796–1807*, 2005.

[44] Frédéric Kuznik, Joseph Virgone, and Kevyn Johannes. Development and validation of a new trnsys type for the simulation of external building walls containing pcm. *Energy and Buildings 42 (2010) 1004–1009*, 2010.

[45] B.L. Gowreesunker, S.A. Tassou, and M. Kolokotroni. Improved simulation of phase change processes in applications where conduction is the dominant heat transfer mode. *Energy and Buildings 47 (2012) 353–359*, 2012.

[46] M.A. Izquierdo-Barrientos, J.F. Belmonte, D. Rodríguez-Sánchez, A.E. Molina, and J.A. Almendros-Ibáñez. A numerical study of external building walls containing phase change materials (pcm). *Applied Thermal Engineering 47 (2012) 73e85*, 2012.

[47] Dariusz Heim and Joe A. Clarke. Numerical modeling and thermal simulation of pcm–gypsum composites with esp-r. *Energy and Buildings 36 (2004) 795–805*, 2004.

[48] D. A. Neeper. Thermal dynamics of wallboard with latebt heat storage. *Solar Energy Vol. 68, No. 5, p. 393-403*, 2000.

[49] Piia Lamberg, Reijo Lehtiniemi, and Anna-Maria Henell. Numerical and experimental investigation of melting and freezing processes in phase change material storage. *International Journal of Thermal Sciences 43 (2004) 277–287*, 2004.

[50] Haitian Yang and Yiqian He. Solving heat transfer problems with phase change via smoothed effective heat capacity and element-free galerkin methods. *International Communications in Heat and Mass Transfer 37 (2010) 385–392*, 2010.

[51] Parham A.Mirzaei and Fariborz Haghighat. Modeling of phase change materials for applications in whole building simulation. *Renewable and Sustainable Energy Reviews 16 (2012) 5355–5362*, 2012.

[52] Per Freiesleben Hansen. *The Science of Construction Materials.* Springer Heidelberg Dordrecht London New York, 2009.

[53] Ksenofon Kakatsios. *Principles of Heat and Mass Transfer.* SYMEON Publishing (greek edition), 2006.

[54] Capobianchi Massimo and Aziz A. Laminar natural convection from an isothermal vertical surface to pseudoplastic and dilatant fluids. *Journal of hear transfer,2012, vol. 134, no12*, 2012.

[55] Hans Dieter Baehr and Karl Stephan. *Heat and Mass Transfer*. Springer, Third Edition, 2011.

[56] The GreenSpec Team. http://www.greenspec.co.uk/energy–efficient–windows.php. Retrieved January 2014.

[57] Georgios Bergeles. *Computational Fluid Dyanmics*. Symeon Publications, Greek Edition, Athens, 2009.

[58] Dimitrios Prigkipas. [2012]. *On the development of computational tool for the simulation of fluid characteristic with concurrent energy storage*, Master thesis, National Technical University of Athens, Greece.

[59] The NETZSCH group. https://www.netzsch-thermal-analysis.com/us/materials-applications/polymers/polycarbonate-thermal-conductivity.html. Retrieved January 2014.

[60] ANSYS. *CFX Documentation*.